

SUPPORTING INFORMATION

Embedding Alkenes within an Icosahedral Inorganic Fullerene {(NH₄)₄₂[Mo₁₃₂O₃₇₂(L)₃₀(H₂O)₇₂]} for Trapping Volatile Organics

Robert W. Pow, Weimin Xuan, De-Liang Long, Nicola L. Bell, and Leroy Cronin*

School of Chemistry, University of Glasgow, University Avenue, Glasgow, G12 8QQ, United Kingdom

Contents

(1) Previously Reported Structures.....	3
(2) Materials and Methods.....	4
CHN Microanalysis.....	4
Nuclear Magnetic Resonance Spectroscopy	4
Single Crystal X-Ray Diffraction.....	4
pH Measurements.....	4
Infrared Spectroscopy	4
Thermogravimetric Analysis.....	4
(3) Synthetic Procedures.....	4
Synthesis of {Mo ₁₃₂ (OAc) ₃₀ } for Ligand-Exchange Syntheses and ¹ H NMR Ligand-Exchange Studies.....	4
Synthesis of {Mo ₁₃₂ (SO ₄) ₃₀ } from {Mo ₁₃₂ (OAc) ₃₀ } for use in Ligand-Exchange Syntheses.....	5
Direct Synthesis of {Mo ₁₃₂ (Acrylic acid)}	5
Ligand-Exchange Syntheses of 1-8 from {Mo ₁₃₂ (SO ₄) ₃₀ }	5
(4) Structural Formulae	6
(5) Thiol Uptake Procedure	7
(6) Infrared Spectroscopy of 1-8.....	7
(7) UV-Vis Spectroscopy of 1-8.....	8
(8) Elemental Analysis of 1-8.....	9
(9) Crystallographic Data of 1, 2, and 5	9
(10) Characterization of 1 – {Mo ₁₃₂ (Acrylic acid)}.....	12
(10.1) Thermogravimetric Analysis of 1	13

(10.2) NMR Study of 1	13
(11) Characterization of 2 – {Mo ₁₃₂ (Crotonic acid)}	17
(11.1) Thermogravimetric analysis of 2	17
(11.2) NMR Study of 2	18
(12) Characterization of 3 – {Mo ₁₃₂ (Methacrylic acid)}	20
(12.1) Thermogravimetric Analysis of 3	20
(12.2) NMR Study of 3	20
(13) Characterization of 4 – {Mo ₁₃₂ (Tiglic acid)}	22
(13.1) Thermogravimetric Analysis of 4	22
(13.2) NMR Study of 4	23
(14) Characterization of 5 – {Mo ₁₃₂ (3-Butenoic acid)}	25
(14.1) Thermogravimetric Analysis of 5	26
(14.2) NMR Study of 5	26
(15) Characterization of 6 – {Mo ₁₃₂ (4-Pentenoic acid)}	29
(15.1) Thermogravimetric Analysis of 6	29
(15.2) NMR Study of 6	29
(16) Characterization of 7 – {Mo ₁₃₂ (5-Hexenoic Acid)}	31
(16.1) Thermogravimetric Analysis of 7	31
(16.2) NMR Study of 7	32
(17) Characterization of 8 – {Mo ₁₃₂ (Sorbic Acid)}	34
(17.1) Thermogravimetric Analysis of 8	34
(17.2) NMR Study of 8	34
(18) Thiol-containing Guest Uptake	36
Investigation of Uptake between Pure {Mo ₁₃₂ (SO ₄) ₃₀ }, {Mo ₁₃₂ (SO ₄) ₃₀ } plus acetic acid, and {Mo ₁₃₂ (SO ₄) ₃₀ } plus alkene ligands, with Thiol-Containing Alkyl Guests	36
Investigation of Increasing Temperature on Uptake of 1-butanethiol with {Mo ₁₃₂ (SO ₄) ₃₀ } plus 3-butenic acid	46
References	50

(1) Previously Reported Structures

Table S1 Reported {Mo₁₃₂} ligands and their associated counterions.

Ligand	Structure	Counterions
Acetate		NH ₄ ⁺ [1] Na ⁺ /DMA ⁺ ^c [4]
		NH ₄ ⁺ /DODA ⁺ ^a [2] Na ⁺ /MimAm ⁺ ^d [5]
		NH ₄ ⁺ /MimCa ⁺ ^b [3]
Sulfate		NH ₄ ⁺ [3] NH ₄ ⁺ /Pr ³⁺ [7] NH ₄ ⁺ /Formadinium [9] NH ₄ ⁺ /Formadinium/ Gd ³⁺ [11] Na ⁺ /Urea-H ⁺ [6]
		NH ₄ ⁺ /Cs ⁺ [6] NH ₄ ⁺ /Li ⁺ [8] NH ₄ ⁺ /Ca ²⁺ / Formadinium [9] NH ₄ ⁺ /Urea-H ⁺ [12] Li ⁺ /DMA ⁺ [8]
		NH ₄ ⁺ /Ce ⁺ [6] NH ₄ ⁺ /DODA ⁺ NH ₄ ⁺ /Formadinium/ Pr ³⁺ [10] NH ₄ ⁺ /Urea-H ⁺ /Ca ²⁺ [12] DMA ⁺ /Al ³⁺ [13]
Phosphate		NH ₄ ⁺ [6] NH ₄ ⁺ /Na ⁺ [6]
Acetate/Sulfate mix		NH ₄ ⁺ [14] Na ⁺ /DMA ⁺ [14]
Sulfate/Phosphate mix		Guanadinium [6]
Formate		NH ₄ ⁺ [15] Formadinium [15]
Carbonate		NH ₄ ⁺ [16] NH ₄ ⁺ /Formadinium [16]
Oxalate		NH ₄ ⁺ [17]
Propanoate		NH ₄ ⁺ [18]
Butyrate		NH ₄ ⁺ [19]
iso-Propanoate		Na ⁺ [20]
tert-Butyrate		Na ⁺ [20]
L-Tartrate		NH ₄ ⁺ [21] NH ₄ ⁺ /DMA ⁺ [21] TBA ⁺ ^e [21]
D-Tartrate		NH ₄ ⁺ [21] DMA ⁺ [21]
Succinate		NH ₄ ⁺ [22] NH ₄ ⁺ /DMA ⁺ [22]
Glutarate		NH ₄ ⁺ [22] NH ₄ ⁺ /DMA ⁺ [22]

^a Dioctadecyl-dimethyl ammonium. ^b 1-methyl-3-alkylimidazolium (where, *n* = 12, 14, 16, 18, 20). ^c Dimethyl ammonium.

^d 3-aminoethyl-1-methylimidazolium. ^e *n* (tetrabutyl ammonium).

(2) Materials and Methods

All chemicals and solvents were used as purchased without further purification.

CHN Microanalysis: Carbon, nitrogen and hydrogen content were determined by the microanalysis services within the School of Chemistry, University of Glasgow using an EA 1110 CHNS, CE-440 Elemental Analyzer.

Nuclear Magnetic Resonance Spectroscopy: ^1H NMR spectra were recorded on a Bruker Ascend Aeon 600 MHz NMR spectrometer. Samples were analysed in Bruker NMR tubes (5 mm diameter, 7" length). Unless otherwise stated, 1.7×10^{-3} M solutions of the $\{\text{Mo}_{132}\}$ -based structures were prepared by dissolving the relevant sample in D_2O . Where required, a methanesulfonic acid reference solution of concentration 3.4×10^{-2} M (i.e. 20x the concentration of the $\{\text{Mo}_{132}\}$ solution) was prepared and transferred to an external axial reference tube.

Single Crystal X-Ray Diffraction: A suitable single crystal was selected and mounted onto a rubber loop using Fomblin oil. Single-crystal datasets and unit cells were collected at 150(2) K on a Bruker Apex II Quasar diffractometer equipped with a graphite monochromator ($\lambda(\text{Mo}_{\text{K}\alpha}) = 0.71073 \text{ \AA}$) equipped with a microfocus X-ray source (50 kV, 1.0 mA) or at Diamond Light Source on Beamline I19 under proposal MT18953. Data collection and reduction were performed using the Apex2 software package and structure solution and refinement were carried out with SHELXS-97²³ and SHELXL-97²⁴ or later version via WinGX²⁵. All of the non-hydrogen atoms (including those disordered) were anisotropically refined. CCDC 1962975-1962977 contains the crystallographic data for structures **1**, **2**, and **5**, and can be obtained free of charge via www.ccdc.cam.ac.uk/data_request/cif, or by emailing data_request@ccdc.cam.ac.uk, or by contacting The Cambridge Crystallographic Data Centre, 12 Union Road, Cambridge, CB2 1EZ, UK; fax: +44 1223 336033.

pH Measurements: Measurements were taken on a Hanna Instruments HI-2210-02 Bench Top pH Meter with pH electrode (HI 1131B) and temperature probe (HI 7662).

Infrared Spectroscopy: All samples were collected in transmission mode using a JASCO FT-IR-410 spectrometer.

Thermogravimetric Analysis: Analysis was performed on a TA Instruments Q 500 Thermogravimetric analyser under nitrogen air flow with a heating rate of $10 \text{ }^\circ\text{C min}^{-1}$ from room temperature ($22 \text{ }^\circ\text{C}$) to $1000 \text{ }^\circ\text{C}$.

(3) Synthetic Procedures

Synthesis of $\{\text{Mo}_{132}(\text{OAc})_{30}\}$ for Ligand-Exchange Syntheses and ^1H NMR Ligand-Exchange Studies¹

Ammonium heptamolybdate tetrahydrate $[(\text{NH}_4)_6\text{Mo}_7\text{O}_{24}\cdot 4\text{H}_2\text{O}]$ (5.6 g, 4.5 mmol) and ammonium acetate $[\text{CH}_3\text{COONH}_4]$ (12.5 g, 162 mmol) were added to a wide-necked 500 mL conical flask containing deionised water (250 mL) and a magnetic stirrer bar. Acetic acid $[\text{CH}_3\text{COOH}]$ (50%) was added, under stirring, until the solution

reached pH 4 (83 mL). Finally, hydrazine sulphate [N₂H₄.H₂SO₄] (0.8 g, 6.1 mmol) was added and the solution was stirred at room temperature for 10 minutes. The resulting dark brown solution was transferred to a crystallisation space (18 °C) and left uncovered to allow solvent evaporation to occur. After 2 days, dark brown hexagonal crystals had formed which were suitable for single-crystal X-ray diffraction data collection – used here to confirm the expected unit cell of the {Mo₁₃₂} structure. The crystals were collected and washed with a minimum amount of ethanol followed by diethyl ether, then dried in air. Yield: 4.04 g (60.6 %, based on Mo).

Synthesis of {Mo₁₃₂(SO₄)₃₀} from {Mo₁₃₂(OAc)₃₀} for use in Ligand-Exchange Syntheses²⁶

{Mo₁₃₂(OAc)₃₀} (4.0 g, 0.14 mmol), prepared as above, and ammonium sulphate [(NH₄)₂SO₄] (16.0 g, 121.1 mmol) were added to a wide-necked 500 mL conical flask containing deionised water (320 mL) and a magnetic stirrer bar. Addition of hydrochloric acid [HCl] (16%), under stirring, produced a solution with pH 1 (16 mL), which was then stirred at 90 °C for 4 hours. After stirring, the dark brown solution was filtered whilst hot, and the filtrate was transferred to the crystallisation room (18 °C) for storage and left uncovered to allow for solvent evaporation to occur. After 4 days, dark brown hexagonal crystals had formed which were suitable for single-crystal X-ray diffraction data collection – used here to confirm the expected unit cell of the {Mo₁₃₂} structure. The crystals were collected and washed with a minimum amount of ethanol followed by diethyl ether, then dried in air. Yield: 1.03 g (25.8 %).

Direct Synthesis of {Mo₁₃₂(Acrylic acid)}

Ammonium heptamolybdate tetrahydrate [(NH₄)₆Mo₇O₂₄.4H₂O] (1.08 g, 1.0 mmol) was added to a 100 mL conical flask containing deionised water (75 mL) and a magnetic stirrer bar. Addition of ammonia solution (25%) (2 mL), acrylic acid (7 mL, 102.0 mmol), and sodium dithionite [Na₂S₂O₄] (85%) (140 mg, 0.8 mmol) followed. The solution was stirred at room temperature for 12 hours, followed by filtration to remove the small amount of precipitate which had formed in the dark brown solution. The resulting solution was covered with parafilm and kept in storage (18 °C). After 2 days, the formation of a small amount of precipitate was removed again by filtration, and the solutions were sealed using parafilm for storage (18 °C). After a further 7 days, dark brown hexagonal crystals formed which were suitable for X-ray diffraction studies. The crystals were collected and washed with a minimum amount of ethanol followed by diethyl ether, then left to dry in air. Yield = 0.17 g (11.5 %, based on Mo).

Ligand-Exchange Syntheses of 1-8 from {Mo₁₃₂(SO₄)₃₀}

{Mo₁₃₂(SO₄)₃₀} (230 mg, 8.0 x 10⁻³ mmol), prepared as above, was added to a wide-necked 50 mL conical flask containing deionised water (15 mL) and a magnetic stirrer bar. The desired ligand for use in each reaction (**Figure S1**) was added in the following amounts: crotonic acid (**2**) – 645 mg, 7.5 mmol (750 eq.), methacrylic acid (**3**) – 160 mg (150 μL), 1.8 mmol (180 eq.), tiglic acid (**4**) – 120 mg, 1.2 mmol (150 eq.), 3-butenic acid (**5**) – 172 mg (169 μL), 2.0 mmol (250 eq.), 4-pentenoic acid (**6**) – 200 mg (204 μL), 2.0 mmol (250 eq.), 5-hexenoic acid (**7**) – 137 mg (140 μL), 1.2 mmol (150 eq.), and sorbic acid (**8**) – 134 mg, 1.2 mmol (150 eq.). The number of equivalents in brackets is the approximate number of equivalents of ligand added in comparison to the number of moles of {Mo₁₃₂(SO₄)₃₀}.

After stirring at 50 °C for 3 days, ammonium chloride (NH₄Cl) – 230 mg, 4.3 mmol, was added and the solutions were stirred for a further 10 mins. The solutions were then transferred to the crystallisation room (18 °C) for storage in their uncovered containers, to allow solvent evaporation to occur. Dark brown, hexagonal crystals which were suitable for single-crystal X-ray analysis appeared after a period of 4 days. The crystals were washed with a minimum amount of ethanol followed by diethyl ether, then dried in air. Yield = 70-90 mg (30-40%).

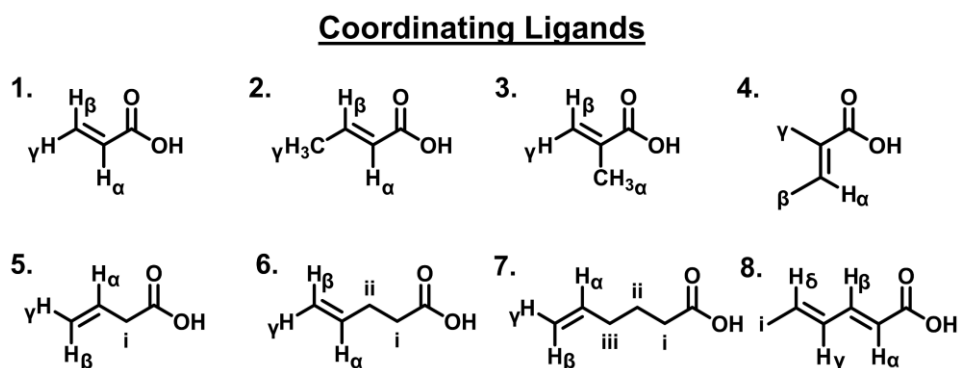
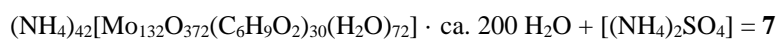
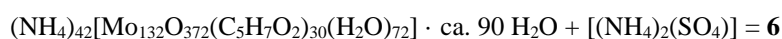
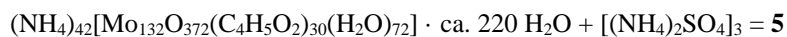
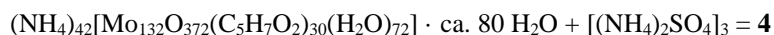
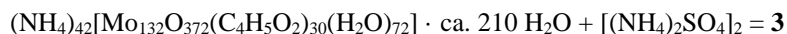
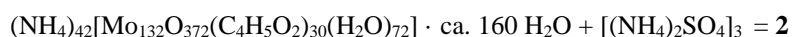
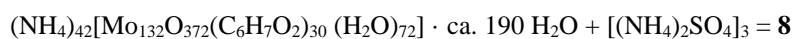


Figure S1: Ligands used for the synthesis of **1-8**: acrylic acid (**1**), crotonic acid (**2**), methacrylic acid (**3**), tiglic acid (**4**), 3-butenic acid (**5**), 4-pentenoic acid (**6**), 5-hexenoic acid (**7**), and sorbic acid (**8**). Analysis of NMR spectra throughout the Supporting Information refers to the labelling of protons as indicated here. In the case of ¹³C NMR studies the relevant carbon nuclei are labelled unambiguously.

(4) Structural Formulae





(5) Thiol Uptake Procedure

$\{\text{Mo}_{132}(\text{SO}_4)_{30}\}$ (50 mg, 1.7×10^{-3} mmol), prepared as above, was dissolved in D_2O (0.6 mL) and added to an NMR tube (5 mm diameter, 7" length). Ligands and thiol guests were added, with shaking, with concentrations as a factor of a specific number of equivalents in comparison to the concentration of the $\{\text{Mo}_{132}(\text{SO}_4)\}$ (described explicitly in the relevant text). After 1 minute the samples were ready to be analyzed via NMR.

(6) Infrared Spectroscopy of 1-8

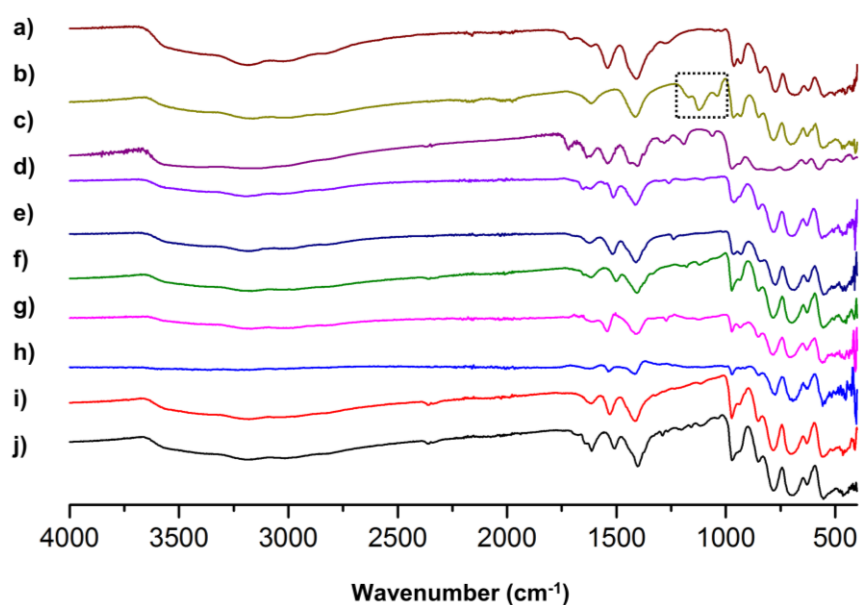


Figure S2: IR spectra for a) $\{\text{Mo}_{132}(\text{OAc})_{30}\}$, b) $\{\text{Mo}_{132}(\text{SO}_4)_{30}\}$, c) **1**, d) **2**, e) **3**, f) **4**, g) **5**, h) **6**, i) **7**, and j) **8**. The triplet due to splitting of the ν_3 stretching mode of the bidentate SO_4^{2-} ligands (C_{2v}) in the 1030-1190 cm^{-1} range, for $\{\text{Mo}_{132}(\text{SO}_4)_{30}\}$, is highlighted by the dashed black box.

(7) UV-Vis Spectroscopy of 1-8

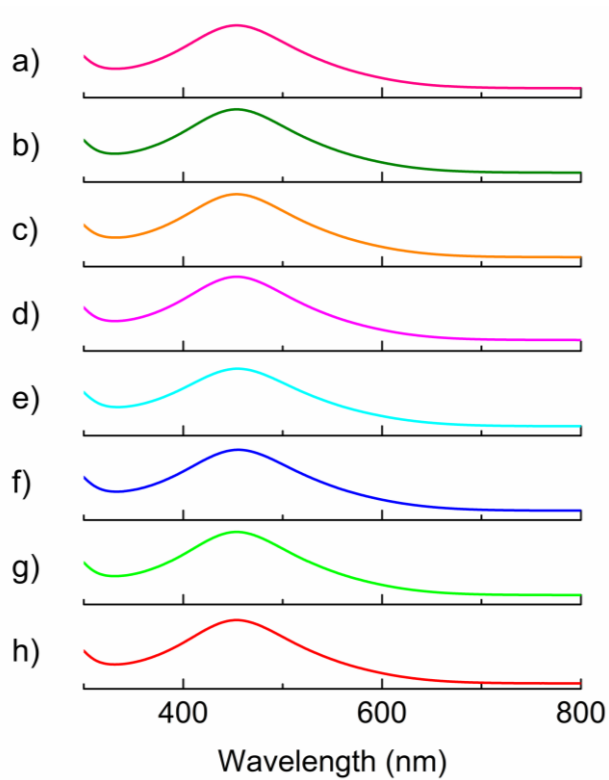


Figure S3: UV-Vis spectra for a) **1**, b) **2**, c) **3**, d) **4**, e) **5**, f) **6**, g) **7**, and h) **8**.

(8) Elemental Analysis of 1-8

Table S2 C, H, N, Mo, and S analysis for products **1-8**. All Values are given as percentages.

STRUCTURE	C	H	N	Mo	S
1	5.59	2.76	2.78	48.07	0.23
2	5.96	2.74	2.85	48.50	0.37
3	6.45	2.89	2.11	46.90	0.50
4	6.08	2.96	2.65	47.55	0.90
5	4.75	2.96	3.94	47.30	0.35
6	6.62	3.05	2.49	46.00	0.13
7	6.80	3.17	2.15	48.28	0.17
8	6.10	2.96	2.33	44.23	0.90

(9) Crystallographic Data of 1, 2, and 5

Table S3 Crystallographic data of **1** – {Mo₁₃₂(Acrylic Acid)}

Identification code	1	
Empirical formula	C114 H810 Mo132 N46 O708 S2	
Formula weight	26886.23	
Temperature (K)	150(2)	
Wavelength (Å)	0.71073	
Crystal system	Trigonal	
Space group	R-3	
Unit cell dimensions	a = 32.6262(18) Å	α = 90°
	b = 32.6262(18) Å	β = 90°
	c = 73.225(5) Å	γ = 120°
Volume (Å ³), Z	67503(9), 3	
Density (calculated) (mg/m ³)	1.984	
Absorption coefficient (mm ⁻¹)	1.879	
F(000)	39168	
Crystal size (mm ³)	0.100 x 0.100 x 0.100	
θ range for data collection (°)	1.927 to 26.000	
Limiting indices	-40 ≤ h ≤ 39, -40 ≤ k ≤ 40, -90 ≤ l ≤ 90	
Reflections collected	197269	
Independent reflections	29487 [R(int) = 0.0344]	
Completeness to theta	25.242°/99.9%	
Absorption correction	Empirical	
Max. and min. transmission	0.426 and 0.328	
Refinement method	Full-matrix least-squares on F ²	
Data / restraints / parameters	29487 / 147 / 1400	
Goodness-of-fit on F ²	1.152	
Final R indices [I > 2σ(I)]	R1 = 0.0591, wR2 = 0.1527	
R indices (all data)	R1 = 0.0775, wR2 = 0.1884	
Extinction coefficient	n/a	
Largest diff. peak and hole (e. Å ⁻³)	2.09 and -1.19	

Table S4 Crystallographic data of **2** – {Mo₁₃₂(Crotonic acid)}

Identification code	2
Empirical formula	C120 H806 Mo 132 N48 O676 S3
Formula weight	26502.34
Temperature (K)	150(2)
Wavelength (Å)	0.6889
Crystal system	Trigonal
Space group	R-3
Unit cell dimensions	a = 32.3898(3) Å $\alpha = 90^\circ$
	b = 32.3898(3) Å $\beta = 90^\circ$
	c = 72.8225(7) Å $\gamma = 120^\circ$
Volume (Å ³), Z	66162.6(14), 3
Density (calculated) (mg/m ³)	1.995
Absorption coefficient (mm ⁻¹)	1.915
F(000)	38586
Crystal size (mm ³)	0.100 x 0.100 x 0.050
θ range for data collection (°)	1.433 to 25.535°
Limiting indices	-40 ≤ h ≤ 40, -40 ≤ k ≤ 40, -90 ≤ l ≤ 90
Reflections collected	303957
Independent reflections	30134 [R(int) = 0.0709]
Completeness to theta	25.242°/99.9%
Absorption correction	Semi-empirical from equivalents
Max. and min. transmission	1.000 and 0.508
Refinement method	Full-matrix least-squares on F ²
Data / restraints / parameters	30134 / 30 / 1429
Goodness-of-fit on F ²	1.082
Final R indices [I > 2σ(I)]	R1 = 0.0640, wR2 = 0.2086
R indices (all data)	R1 = 0.0698, wR2 = 0.2176
Extinction coefficient	0.000033(2)
Largest diff. peak and hole (e. Å ⁻³)	1.69 and -1.03

Table S5 Crystallographic data of **5** – {Mo₁₃₂(3-Butenoic acid)}

Identification code	5
Empirical formula	C120 H926 Mo132 N48 O736 S3
Formula weight	27583.29
Temperature (K)	150(2)
Wavelength (Å)	0.6889
Crystal system	Trigonal
Space group	R-3
Unit cell dimensions	a = 32.4465(2) Å $\alpha = 90^\circ$
	b = 32.4465(2) Å $\beta = 90^\circ$
	c = 72.8870(5) Å $\gamma = 120^\circ$
Volume (Å ³), Z	66453.3(9), 3
Density (calculated) (mg/m ³)	2.068
Absorption coefficient (mm ⁻¹)	1.916
F(000)	40386
Crystal size (mm ³)	0.100 x 0.100 x 0.030
θ range for data collection (°)	1.463 to 25.537°.
Limiting indices	-40<=h<=40, -40<=k<=40, -91<=l<=91
Reflections collected	301757
Independent reflections	30227 [R(int) = 0.0823]
Completeness to theta	25.242°/99.9%
Absorption correction	Semi-empirical from equivalents
Max. and min. transmission	1.000 and 0.599
Refinement method	Full-matrix least-squares on F ²
Data / restraints / parameters	30227 / 40 / 1465
Goodness-of-fit on F ²	1.066
Final R indices [I>2sigma(I)]	R1 = 0.0598, wR2 = 0.1943
R indices (all data)	R1 = 0.0661, wR2 = 0.2012
Extinction coefficient	0.000024(3)
Largest diff. peak and hole (e. Å ⁻³)	1.79 and -1.16

(10) Characterization of **1** – {Mo₁₃₂(Acrylic acid)}

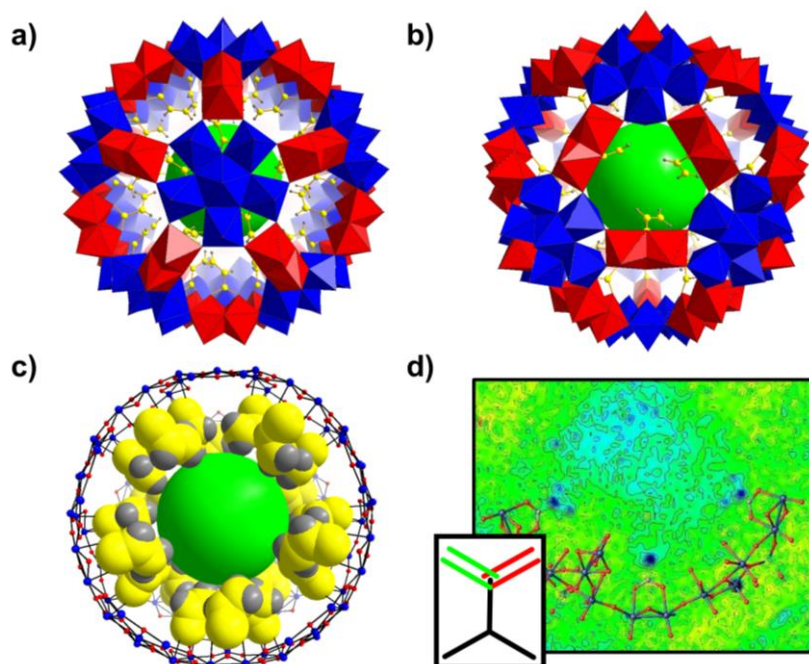


Figure S4: **a)** Polyhedral framework representation of **1** with ball-and-stick acrylic acid ligands, viewed along one of the 12 pentagonal {(Mo)Mo₅} units, **b)** polyhedral framework representation of **1** with ball-and-stick acrylic acid ligands, viewed along one of the 20 {Mo₉O₉} pores, **c)** ball-and stick framework representation of **1** with space-filling acrylic acid ligands, with one pentagonal unit and 5 {Mo₂} units and all non-coordinating oxygen atoms removed for clarity, **d)** electron density map of **1** with a partial section of the framework and ligand atoms shown, with emphasis of the two distinct orientations of the acrylic acid ligand, as a result of rotational isomerization, shown in the inset. For **a)**-**c)**, a green sphere has been added to fill the central cavity. Key: polyhedra – red = {Mo₂} linker-type units, blue = {(Mo)Mo₅} pentagonal-type units; atoms - red = oxygen, blue = molybdenum, yellow = carbon, grey = hydrogen; electron density – blue = high, and green = low electron density.

(10.1) Thermogravimetric Analysis of **1**

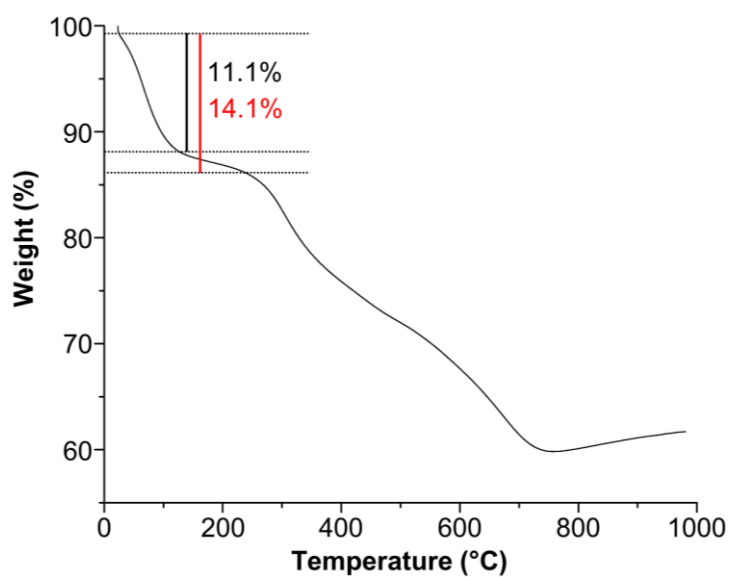


Figure S5: TGA of **1**. The percentage weight loss due to water loss between 50-225 °C is highlighted, representing approximately 180 solvent molecules.

(10.2) NMR Study of **1**

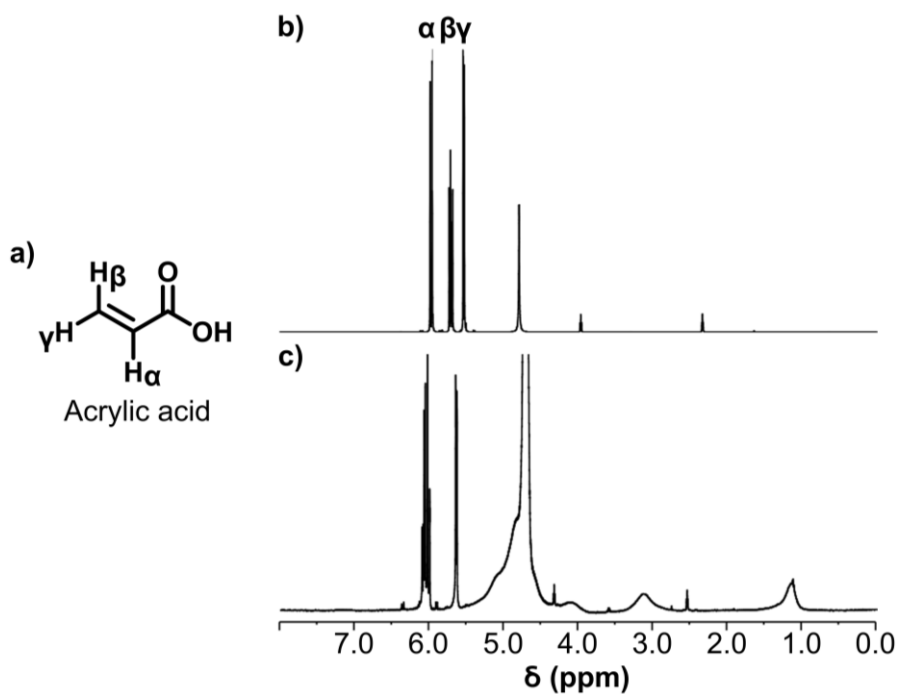


Figure S6: a) Structure of acrylic acid with labelled proton groups, b) ¹H NMR spectrum of acrylic acid in D₂O, and c) ¹H NMR spectrum of **1** in D₂O. The peaks arising from the solvated acrylic acid ligand species are highlighted: α

= 5.9 ppm, β = 5.7 ppm, and γ = 5.5 ppm. The encapsulated acrylic acid ligand species cannot be resolved due to overlapping signals between the water peak and the encapsulated species, at approximately 4.5-5.5 ppm. In addition, impurity peaks are present at 4.0 ppm and 2.4 ppm (for the free ligand), with related broad peaks at 3.2 ppm and 1.2 ppm. Using additional NMR techniques, presented in the SI, the impurity was determined to be the acrylic acid dimer, 3-(acryloyloxy)propanoic acid, which is known to form spontaneously in stored solutions of acrylic acid.²⁷

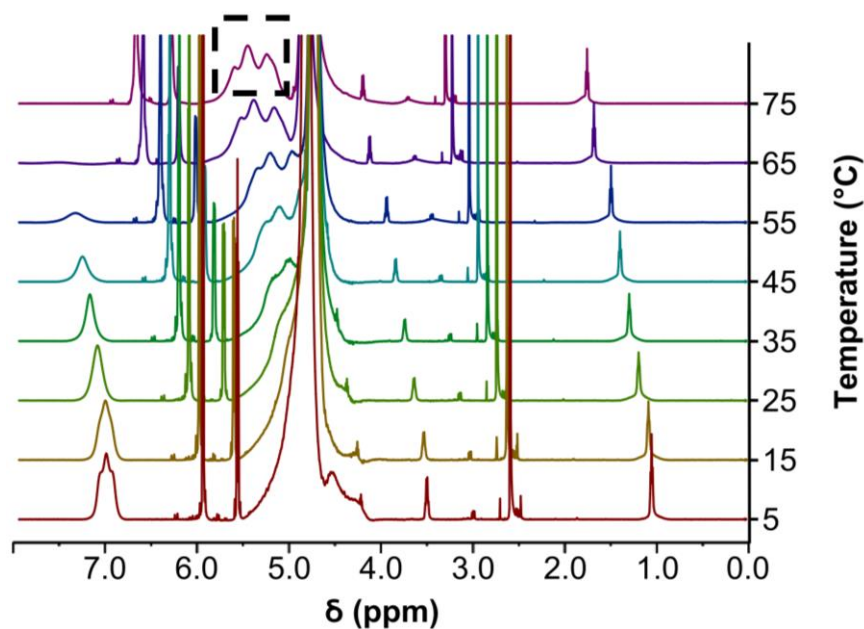


Figure S7: Variable-temperature (5-75 °C) ¹H NMR spectrum of **1** in D₂O. The peaks previously ‘hidden’ by the water peak at room temperature measurements are effectively separated from this position and appear distinct from that of the water peak at temperatures greater than 45 °C (highlighted by the dashed box), between 5.5 ppm and 5.1 ppm.

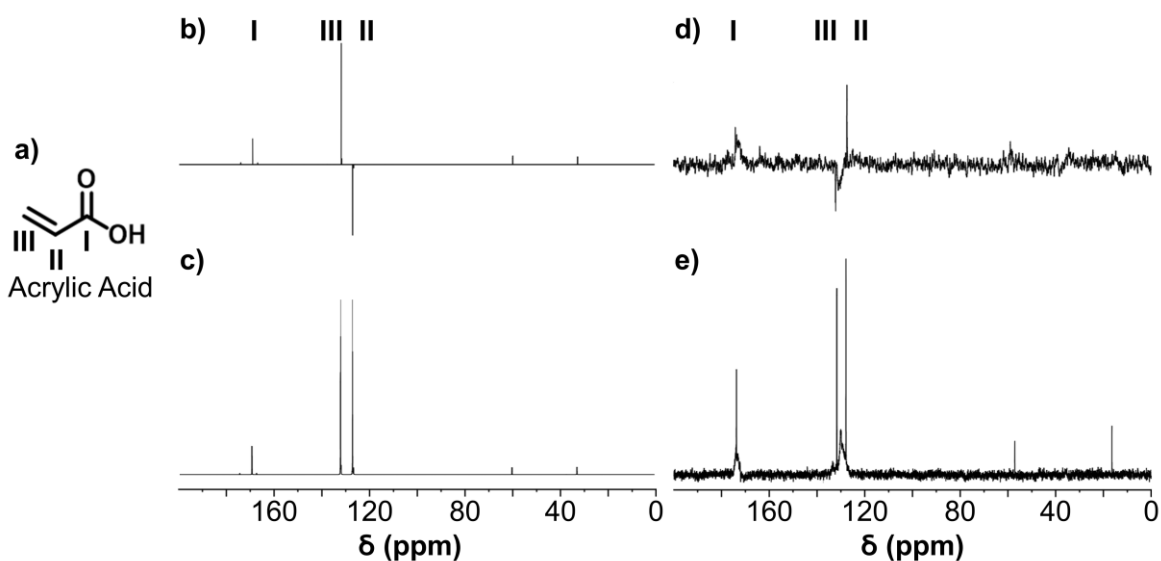


Figure S8: a) Assignment of acrylic acid for use in ^{13}C NMR spectra labelling, b) ^{13}C DEPTQ NMR spectrum of acrylic acid in D_2O , c) ^{13}C NMR spectrum of acrylic acid in D_2O , d) ^{13}C DEPTQ NMR spectrum of **1** in D_2O , and e) ^{13}C NMR spectrum of **1** in D_2O . For the ^{13}C DEPTQ NMR measurements signals arising due to quaternary carbon nuclei (C_q) and methylene (CH_2) carbon nuclei appear pointing upwards, whilst methine (CH) and methyl (CH_3) carbon nuclei appear pointing downwards. The peaks arising from the solvated acrylic acid ligand species are highlighted: **I** = 170 ppm ($-\text{COO}^-$), **II** = 127 ppm ($-\text{CH}$), and **III** = 133 ppm ($-\text{CH}_2$). The encapsulated acrylic acid ligand species appear slightly shifted and broadened due to the same effects expressed in the ^1H NMR spectra. In addition, impurity peaks are present at 61 ppm and 33 ppm.

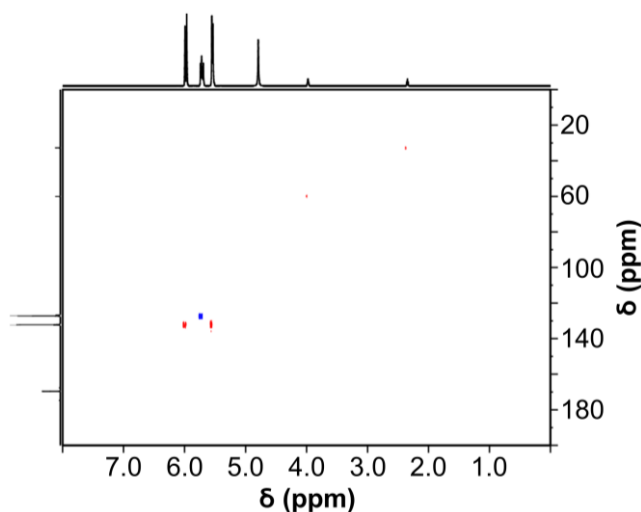


Figure S9: ^1H - ^{13}C multiplicity-edited HSQC 2D NMR spectrum of acrylic acid in D_2O . Here, the CH and CH_3 signals are highlighted as blue, whilst CH_2 signals are highlighted red. The impurity signals (^1H : 4.0 ppm and 2.4

ppm, ^{13}C : 61 ppm and 33 ppm) are therefore assigned as CH_2 groups, confirming the presence of 3-(acryloyloxy)propanoic acid.

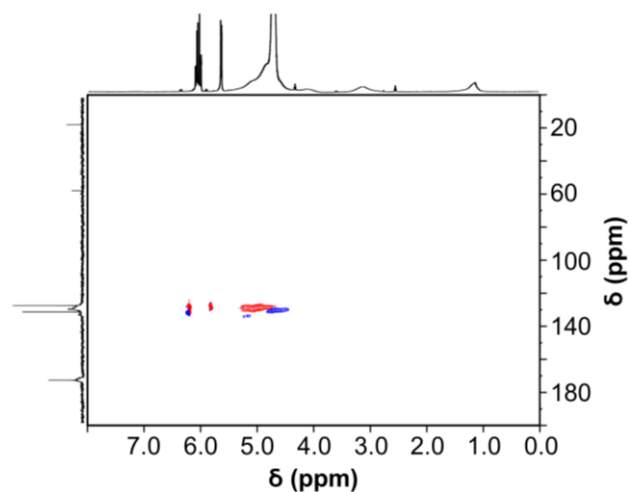


Figure S10: ^1H - ^{13}C multiplicity-edited HSQC 2D NMR spectrum of **1** in D_2O . The broad signals hidden by the water peak, attributed to encapsulated acrylic acid ligands can be partially resolved using this technique.

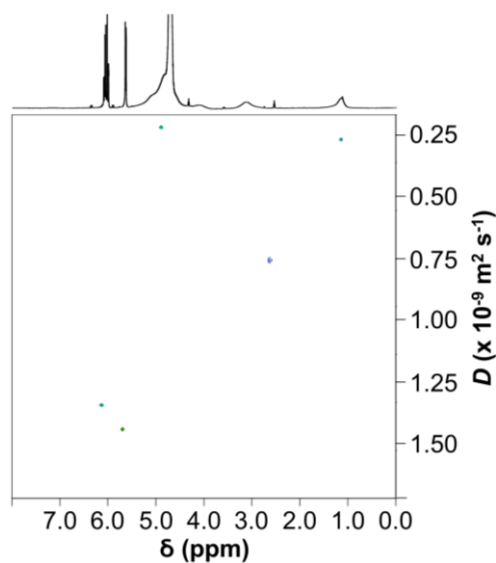


Figure S11: ^1H DOSY NMR spectrum of **1** in D_2O . The signals arising from the solvated acrylic acid ligand species ($\alpha\beta\gamma$) and the encapsulated acrylic acid ligand species are highlighted. The solvated acrylic acid ligands have a diffusion coefficient of approximately $1.40 \times 10^{-9} \text{ m}^2 \text{ s}^{-1}$, whilst the encapsulated acrylic acid signals possess diffusion coefficients of approximately $2.50 \times 10^{-10} \text{ m}^2 \text{ s}^{-1}$. The large discrimination of the two values provides further evidence of their origins from species in two different domains.

(11) Characterization of **2** – {Mo₁₃₂(Crotonic acid)}

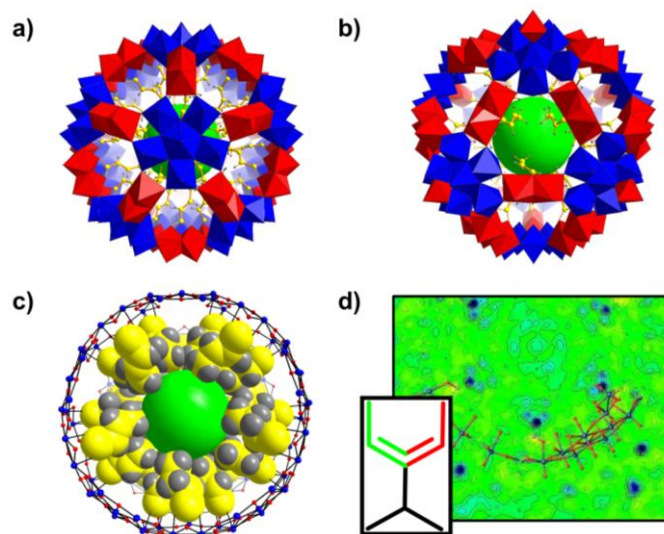


Figure S12: a) Polyhedral framework representation of **2** with ball-and-stick crotonic acid ligands, viewed along one of the 12 pentagonal {(Mo)Mo₅} units, b) polyhedral framework representation of **2** with ball-and-stick crotonic acid ligands, viewed along one of the 20 {Mo₉O₉} pores, c) ball-and stick framework representation of **2** with space-filling crotonic acid ligands, with one pentagonal unit and 5 {Mo₂} units and all non-coordinating oxygen atoms removed for clarity, d) electron density map of **2** with a partial section of the framework and ligand atoms shown, with emphasis of the two distinct orientations of the crotonic acid ligand, as a result of rotational isomerization, shown in the inset. For a)-c), a green sphere has been added to fill the central cavity. Key: polyhedra – red = {Mo₂} linker-type units, blue = {(Mo)Mo₅} pentagonal-type units; atoms - red = oxygen, blue = molybdenum, yellow = carbon, grey = hydrogen; electron density – blue = high, and green = low electron density.

(11.1) Thermogravimetric analysis of **2**

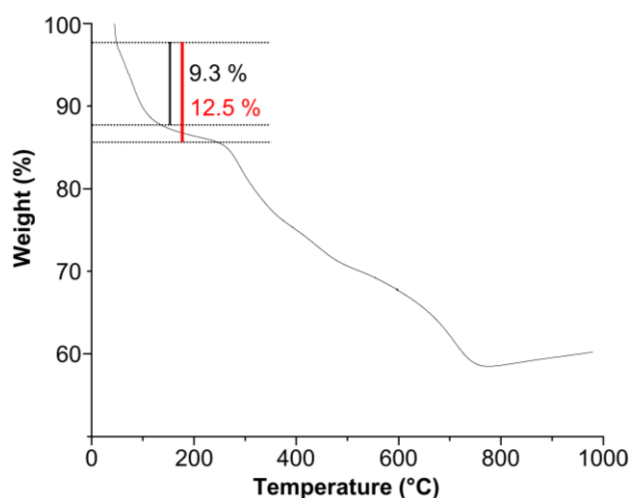


Figure S13: TGA of **2**. The percentage weight loss due to water loss between 50-225 °C is highlighted, representing approximately 160 solvent molecules.

(11.2) NMR Study of 2

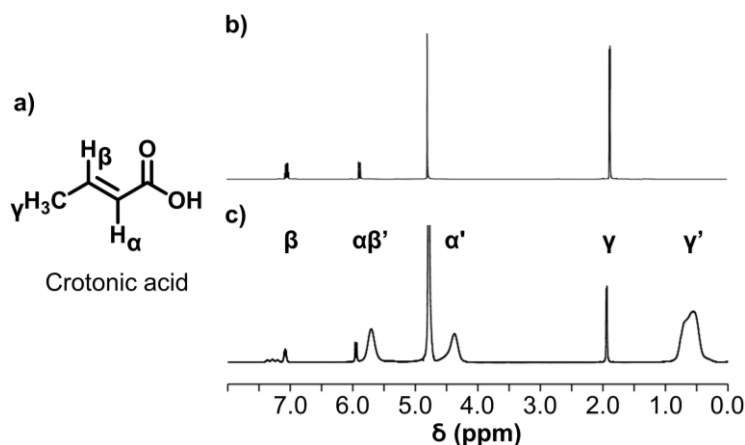


Figure S14: a) Structure of crotonic acid with labelled proton groups b) ^1H NMR spectrum of crotonic acid in D_2O , and c) ^1H NMR spectrum of **2** in D_2O . The peaks arising from the solvated crotonic acid ligand species are highlighted: $\alpha = 5.9$ ppm, $\beta = 7.0$ ppm, and $\gamma = 1.9$ ppm. The encapsulated crotonic acid ligand species peaks appear significantly broadened and upfield shifted due to the coordination of the species to the negatively charged $\{\text{Mo}_{132}\}$, framework in addition to the confined nature of the ligand environment. The resultant peaks appear at $\alpha' = 4.4$ ppm, $\beta' = 5.7$ ppm, and $\gamma' = 0.7$ ppm, with shifts of $\alpha - \alpha' = -1.5$ ppm, $\beta - \beta' = -1.3$ ppm, and $\gamma - \gamma' = -1.2$ ppm.

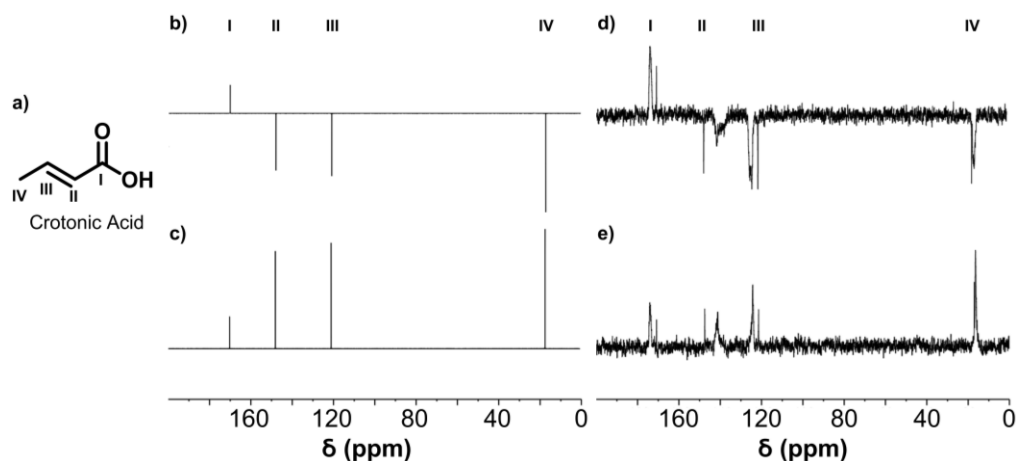


Figure S15: a) Assignment of crotonic acid for use in ^{13}C NMR spectra labelling, b) ^{13}C DEPTQ NMR spectrum of crotonic acid in D_2O , c) ^{13}C NMR spectrum of crotonic acid in D_2O , d) ^{13}C DEPTQ NMR spectrum of **2** in D_2O , and e) ^{13}C NMR spectrum of **2** in D_2O . For the ^{13}C DEPTQ NMR measurements signals arising due to quaternary carbon nuclei (C_q) and methylene (CH_2) carbon nuclei appear pointing upwards, whilst methine (CH) and methyl (CH_3) carbon nuclei appear pointing downwards. The peaks arising from the solvated crotonic acid ligand species are highlighted: **I** = 171 ppm ($-\text{COO}^-$), **II** = 148 ppm ($-\text{CH}$), **III** = 121 ppm ($-\text{CH}$), and **IV** = 17 ppm ($-\text{CH}_3$). The

encapsulated crotonic acid ligand species appear slightly shifted and broadened due to the same effects expressed in the ^1H NMR spectra.

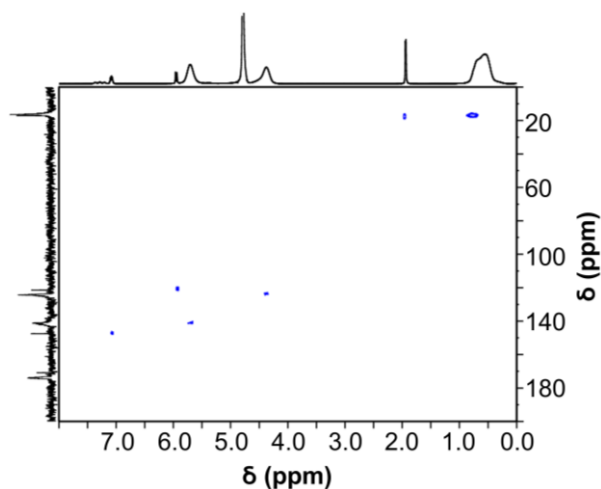


Figure S16: ^1H - ^{13}C multiplicity-edited HSQC 2D NMR spectrum of **2** in D_2O . The CH and CH_3 signals are highlighted as blue. The spectrum confirms the correlation between peaks of the free crotonic acid and their related encapsulated peak signals, in both the ^{13}C and ^1H spectra.

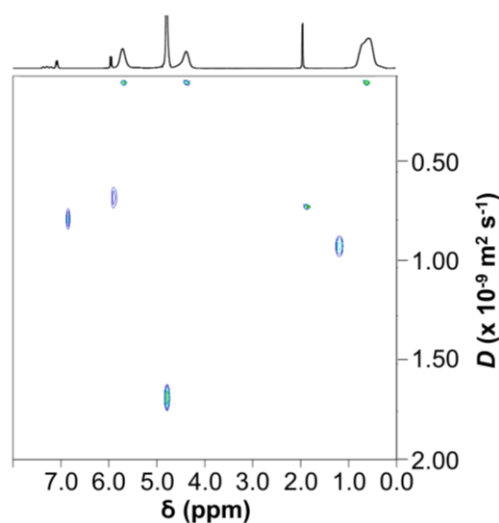


Figure S17: ^1H DOSY NMR spectrum of **2** in D_2O . The signals arising from the solvated crotonic acid ligand species ($\alpha\beta\gamma$) and the encapsulated crotonic acid ligand species ($\alpha'\beta'\gamma'$) are highlighted. The solvated crotonic acid ligands have a diffusion coefficient of approximately $7.62 \times 10^{-10} \text{ m}^2 \text{ s}^{-1}$, whilst the encapsulated crotonic acid signals possess diffusion coefficients of approximately $1.15 \times 10^{-10} \text{ m}^2 \text{ s}^{-1}$. The large discrimination of the two values provides further evidence of their origins from species in two different domains. An additional peak arising from water has a diffusion coefficient of $1.75 \times 10^{-9} \text{ m}^2 \text{ s}^{-1}$. Finally, an impurity peak at 1.1 ppm has a similar diffusion coefficient to the free crotonic acid species, $9.56 \times 10^{-10} \text{ m}^2 \text{ s}^{-1}$.

(12) Characterization of **3** – {Mo₁₃₂(Methacrylic acid)}

(12.1) Thermogravimetric Analysis of **3**

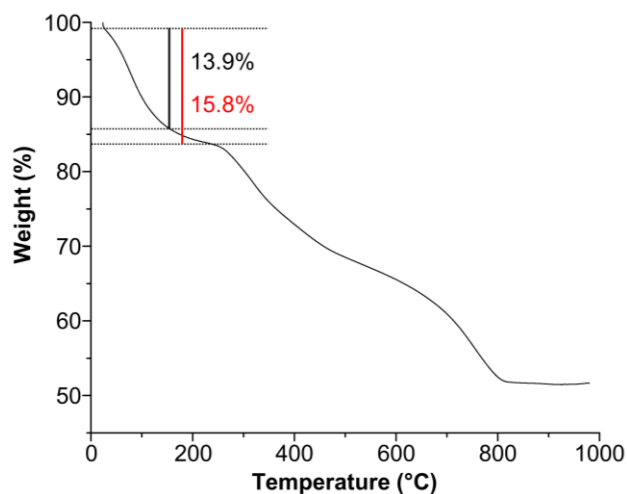


Figure S18: TGA of **3**. The percentage weight loss due to water loss between 50-225 °C is highlighted, representing approximately 210 solvent molecules.

(12.2) NMR Study of **3**

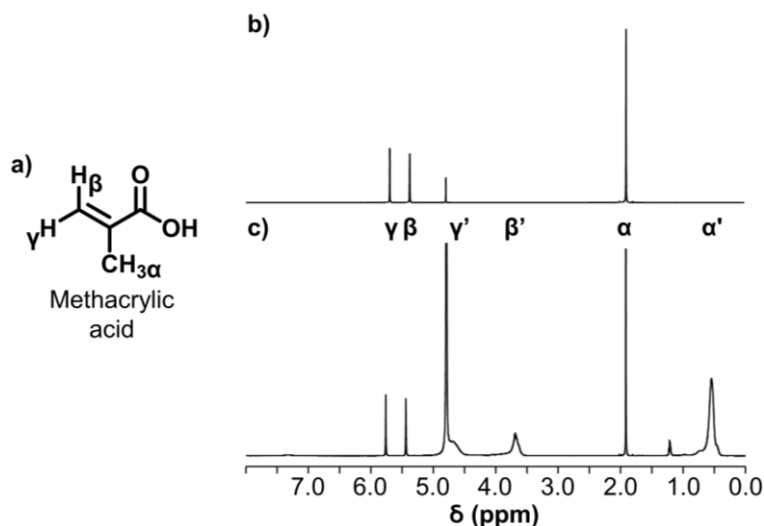


Figure S19: a) Structure of methacrylic acid with labelled proton groups, b) ¹H NMR spectrum of methacrylic acid in D₂O, and c) ¹H NMR Spectrum of **3** in D₂O. The peaks arising from the solvated methacrylic acid ligand species are highlighted: α = 1.9 ppm, β = 5.4 ppm, and γ = 5.7 ppm. The encapsulated methacrylic acid ligand species peaks appear significantly broadened and upfield shifted due to the coordination of the species to the negatively charged

{Mo₁₃₂} framework, in addition to the confined nature of the ligand environment. The resultant peaks appear at α' = 0.6 ppm, β' = 3.7 ppm, and γ' = 4.7 ppm, with shifts of $\alpha-\alpha'$ = -1.3 ppm, $\beta-\beta'$ = -1.7 ppm, and $\gamma-\gamma'$ = -1.0 ppm.

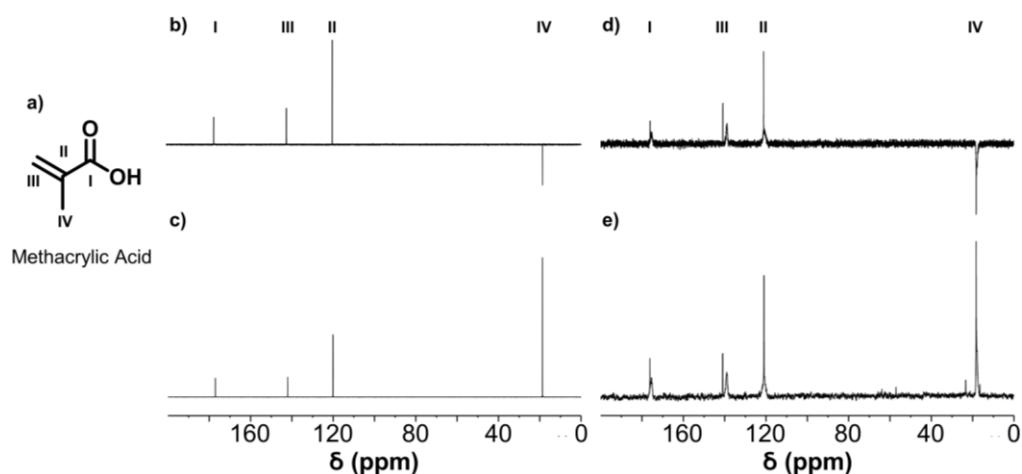


Figure S20: a) Assignment of methacrylic acid for use in ¹³C NMR spectra labelling, b) ¹³C DEPTQ NMR spectrum of methacrylic acid in D₂O, c) ¹³C NMR spectrum of methacrylic acid in D₂O, d) ¹³C DEPTQ NMR spectrum of **3** in D₂O, and e) ¹³C NMR spectrum of **3** in D₂O. For the ¹³C DEPTQ NMR measurements signals arising due to quaternary carbon nuclei (C_q) and methylene (CH₂) carbon nuclei appear pointing upwards, whilst methine (CH) and methyl (CH₃) carbon nuclei appear pointing downwards. The peaks arising from the solvated methacrylic acid ligand species are highlighted: **I** = 177 ppm (-COO⁻), **II** = 121 ppm (-C-), **III** = 142 ppm (-CH₂), and **IV** = 19 ppm (-CH₃). The encapsulated methacrylic acid ligand species peaks appear slightly shifted and broadened due to the same effects expressed in the ¹H NMR spectra.

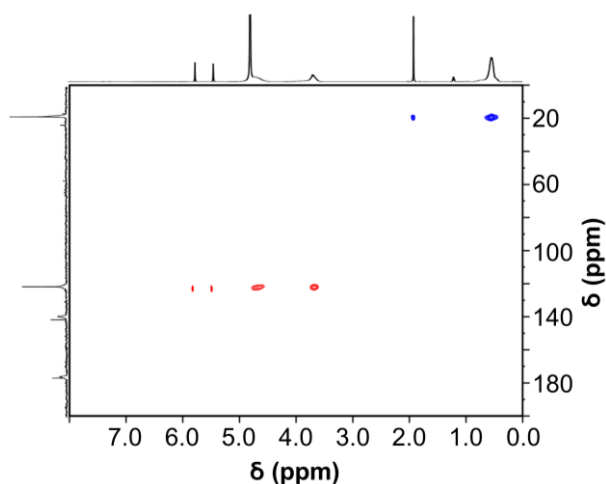


Figure S21: ¹H-¹³C multiplicity-edited HSQC 2D NMR spectrum of **3** in D₂O. Here, CH₃ signals are highlighted in blue, whilst CH₂ signals are highlighted in red. The spectrum confirms the correlation between peaks originating from the free methacrylic acid and the related encapsulated peak signals, in both the ¹³C and ¹H spectra.

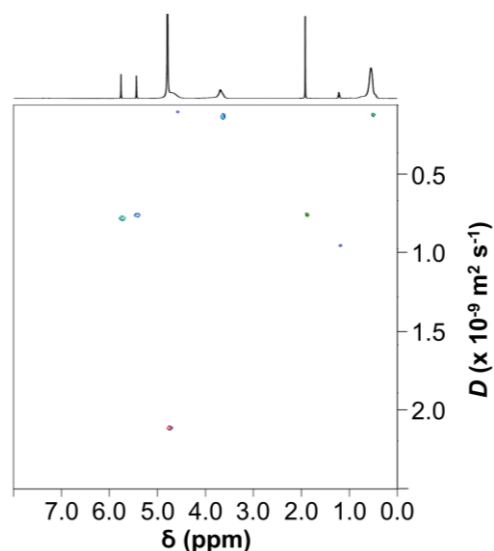


Figure S22: ^1H DOSY NMR spectrum of **3** in D_2O . The signals arising from the solvated methacrylic acid ligand species ($\alpha\beta\gamma$) and the encapsulated methacrylic acid ligand species ($\alpha'\beta'\gamma'$) are highlighted. The solvated methacrylic acid ligands have a diffusion coefficient of approximately $7.58 \times 10^{-10} \text{ m}^2 \text{ s}^{-1}$, whilst the encapsulated methacrylic acid signals possess diffusion coefficients of approximately $1.14 \times 10^{-10} \text{ m}^2 \text{ s}^{-1}$. The large discrimination of the two values provides further evidence of their origins from species in two different domains. An additional peak arising from water has a diffusion coefficient of $2.11 \times 10^{-9} \text{ m}^2 \text{ s}^{-1}$. Finally, an impurity peak at 1.1 ppm has a similar diffusion coefficient to the free methacrylic acid species, $9.49 \times 10^{-10} \text{ m}^2 \text{ s}^{-1}$.

(13) Characterization of **4** – $\{\text{Mo}_{132}(\text{Tiglic acid})\}$

(13.1) Thermogravimetric Analysis of **4**

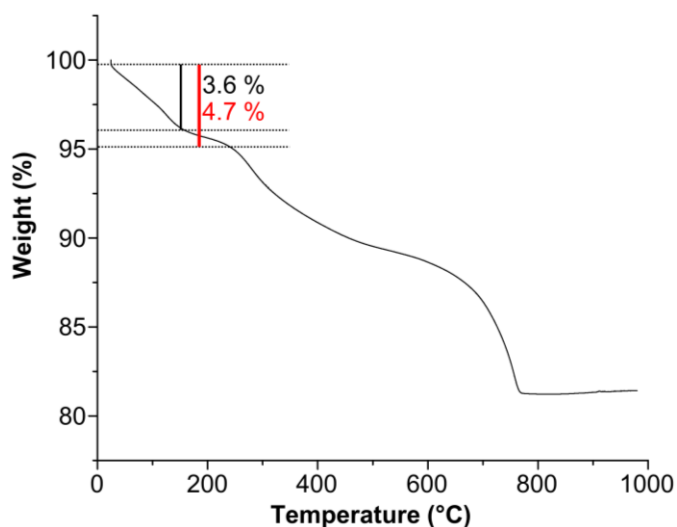


Figure S23: TGA of **4**. The percentage weight loss due to water loss between 50-225 °C is highlighted, representing approximately 80 solvent molecules.

(13.2) NMR Study of **4**

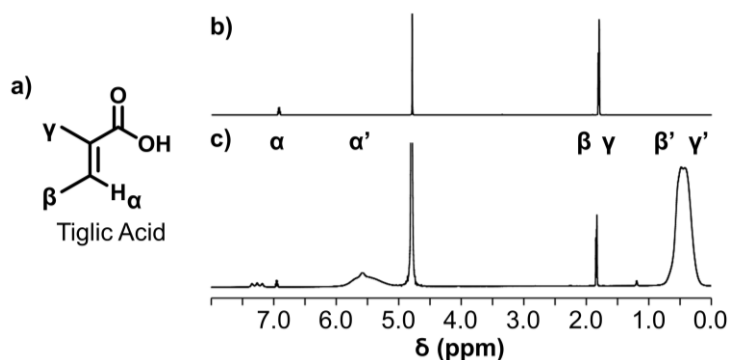


Figure S24: a) Structure of tiglic acid with labelled proton groups, b) ^1H NMR spectrum of tiglic acid in D_2O , and c) ^1H NMR spectrum of **4** in D_2O . The peaks arising from the solvated tiglic acid ligand species are highlighted: α = 6.9 ppm, and β and γ = 1.8 ppm. The encapsulated tiglic acid ligand species peaks appear significantly broadened and upfield shifted due to the coordination of the species to the negatively charged $\{\text{Mo}_{132}\}$ framework, in addition to the confined nature of the ligand environment. The resultant peaks appear at α' = 5.6 ppm, and β' and γ' = 0.4 ppm, with shifts of $\alpha - \alpha' = -1.3$ ppm, and $\beta - \beta'$ and $\gamma - \gamma' = -1.4$ ppm.

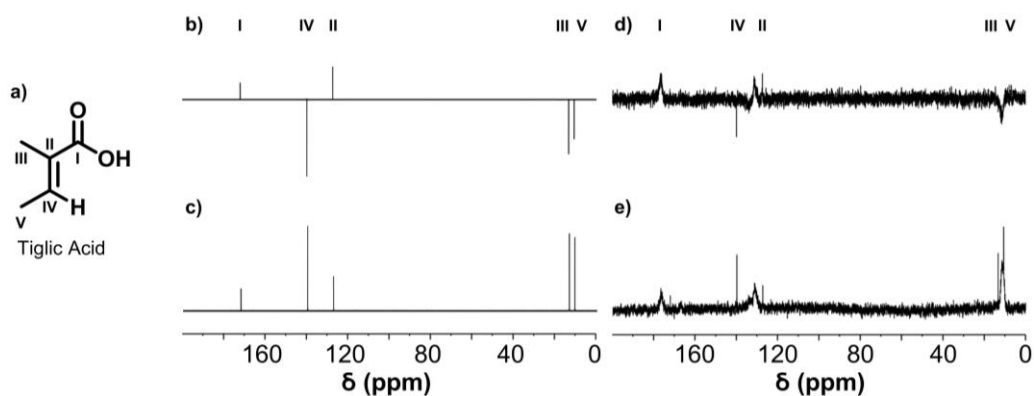


Figure S25: a) Assignment of tiglic acid for use in ^{13}C NMR spectra labelling, b) ^{13}C DEPTQ NMR spectrum of tiglic acid in D_2O , c) ^{13}C NMR spectrum of tiglic acid in D_2O , d) ^{13}C DEPTQ NMR spectrum of **4** in D_2O , and e) ^{13}C NMR spectrum of **4** in D_2O . For the ^{13}C DEPTQ NMR measurements signals arising due to quaternary carbon nuclei (C_q) and methylene (CH_2) carbon nuclei appear pointing upwards, whilst methine (CH) and methyl (CH_3) carbon nuclei appear pointing downwards. The peaks arising from the solvated tiglic acid ligand species are highlighted: **I** = 176 ppm ($-\text{COO}^-$), **II** = 127 ppm ($-\text{C}-$), **III/V** = 10/13 ppm ($-\text{CH}_3$), and **IV** = 140 ppm ($-\text{CH}$). The encapsulated tiglic acid ligand species peaks appear slightly shifted and broadened due to the same effects expressed in the ^1H NMR spectra.

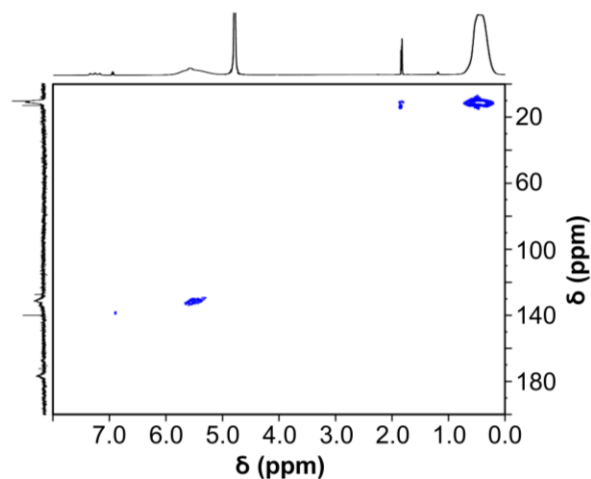


Figure S26: ^1H - ^{13}C multiplicity-edited HSQC 2D NMR spectrum of **4** in D_2O . Here, CH and CH_3 signals are highlighted in blue. The spectrum confirms the correlation between peaks originating from the free tiglic acid and the related encapsulated peak signals, in both the ^{13}C and ^1H spectra.

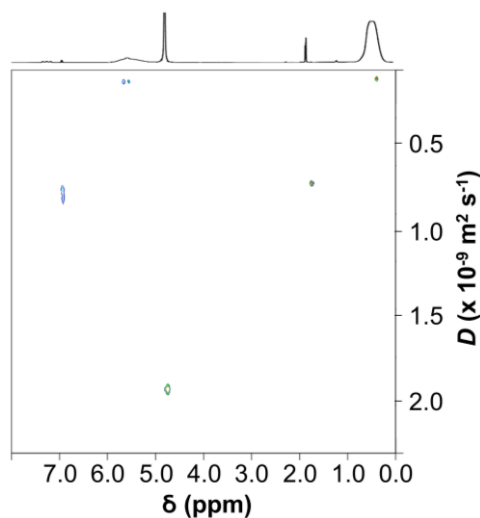


Figure S27: ^1H DOSY NMR spectrum of **4** in D_2O . The signals arising from the solvated tiglic acid ligand species ($\alpha\beta\gamma$) and the encapsulated tiglic acid ligand species ($\alpha'\beta'\gamma'$) are highlighted. The solvated tiglic acid ligands have a diffusion coefficient of approximately $7.51 \times 10^{-10} \text{ m}^2 \text{ s}^{-1}$, whilst the encapsulated tiglic acid signals possess diffusion coefficients of approximately $1.21 \times 10^{-10} \text{ m}^2 \text{ s}^{-1}$. The large discrimination of the two values provides further evidence of their origins from species in two different domains. An additional peak arising from water has a diffusion coefficient of $1.93 \times 10^{-9} \text{ m}^2 \text{ s}^{-1}$.

(14) Characterization of **5** – {Mo₁₃₂(3-Butenoic acid)}

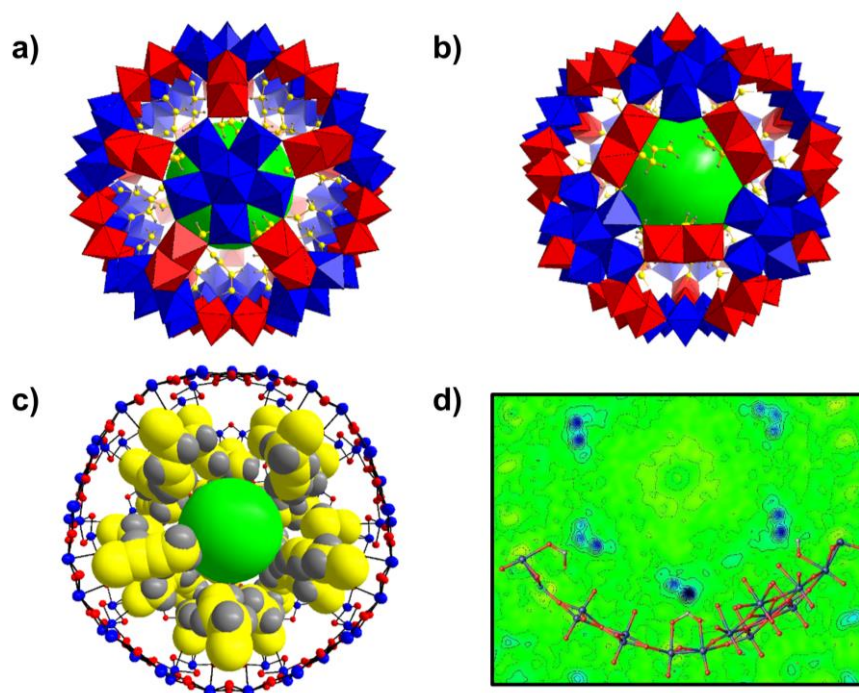


Figure S28: **a)** Polyhedral framework representation of **5** with ball-and-stick 3-butenic acid ligands, viewed along one of the 12 pentagonal {(Mo)Mo₅} units, **b)** polyhedral framework representation of **5** with ball-and-stick 3-butenic acid ligands, viewed along one of the 20 {Mo₉O₉} pores, **c)** ball-and stick framework representation of **5** with space-filling 3-butenic acid ligands, with one pentagonal unit and 5 {Mo₂} units and all non-coordinating oxygen atoms removed for clarity, **d)** electron density map of **5** with a partial section of the framework and ligand atoms shown. For **a)**-**c)**, a green sphere has been added to fill the central cavity. Key: polyhedra – red = {Mo₂} linker-type units, blue = {(Mo)Mo₅} pentagonal-type units; atoms - red = oxygen, blue = molybdenum, yellow = carbon, grey = hydrogen; electron density – blue = high, and green = low electron density.

(14.1) Thermogravimetric Analysis of **5**

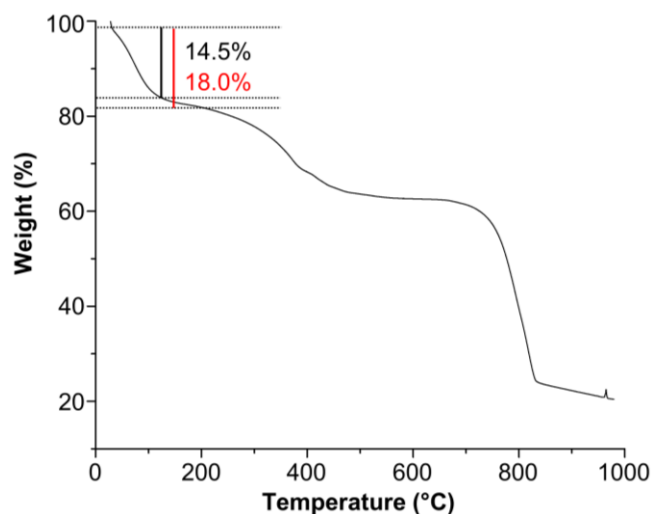


Figure S29: TGA of **5**. The percentage weight loss due to water loss between 50-225 °C is highlighted, representing approximately 220 solvent molecules.

(14.2) NMR Study of **5**

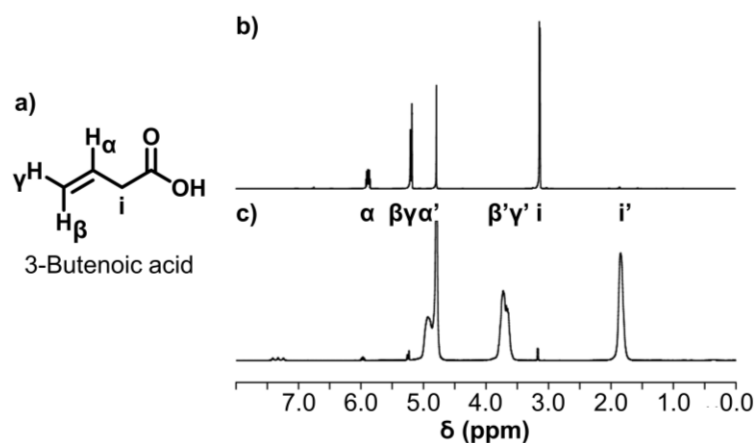


Figure S30: a) Structure of 3-butenoic acid with labelled proton groups, b) ^1H NMR spectrum of 3-butenoic acid in D_2O , and c) ^1H NMR spectrum of **5** in D_2O . The peaks arising from the solvated 3-butenoic acid ligand species are highlighted: $\alpha = 6.0$ ppm, $\beta/\gamma = 5.3$ ppm, and $\text{i} = 3.2$ ppm. The encapsulated 3-butenoic acid ligand species peaks appear significantly broadened and upfield shifted due to the coordination of the species to the negatively charged $\{\text{Mo}_{132}\}$ framework, in addition to the confined nature of the ligand environment. The resultant peaks appear at, $\alpha' = 4.9$ ppm, $\beta'/\gamma' = 3.7$ ppm, and $\text{i}' = 1.8$ ppm, with shifts of $\alpha - \alpha' = -1.1$ ppm, $\beta - \beta'/\gamma - \gamma' = -1.6$ ppm, and $\text{i} - \text{i}' = -1.4$ ppm.

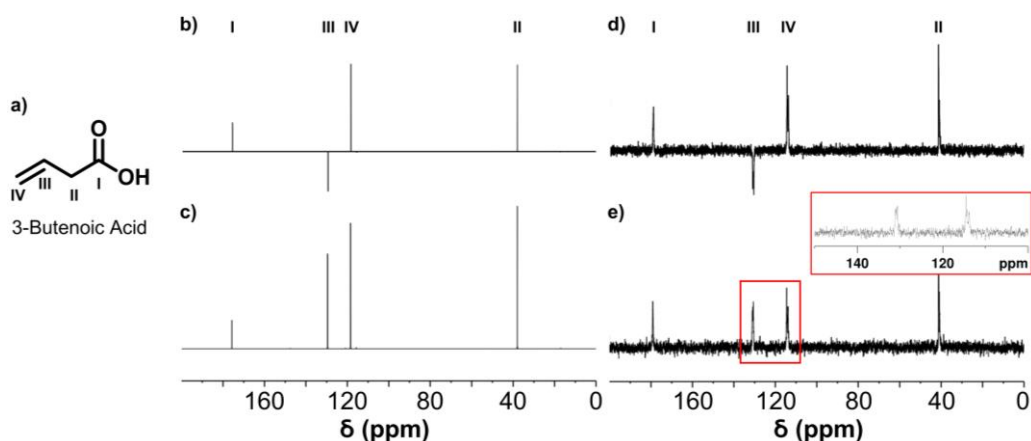


Figure S31: a) Assignment of 3-butenoic acid for use in ^{13}C NMR spectra labelling, b) ^{13}C DEPTQ NMR spectrum of 3-butenoic acid in D_2O , c) ^{13}C NMR spectrum of 3-butenoic acid in D_2O , d) ^{13}C DEPTQ NMR spectrum of **5** in D_2O , and e) ^{13}C NMR spectrum of **5** in D_2O , with expanded section showing broadened resonances relating to ligand coordination shown in the inset. For the ^{13}C DEPTQ NMR measurements signals arising due to quaternary carbon nuclei (C_q) and methylene (CH_2) carbon nuclei appear pointing upwards, whilst methine (CH) and methyl (CH_3) carbon nuclei appear pointing downwards. The peaks arising from the solvated 3-butenoic acid ligand species are highlighted: **I** = 179 ppm ($-\text{COO}^-$), **II** = 40 ppm ($-\text{CH}$), **III** = 130 ppm ($-\text{CH}_2$), and **IV** = 114 ppm ($-\text{CH}_2$). The encapsulated 3-butenoic ligand species appear slightly shifted and broadened due to the same effects expressed in the ^1H NMR spectra.

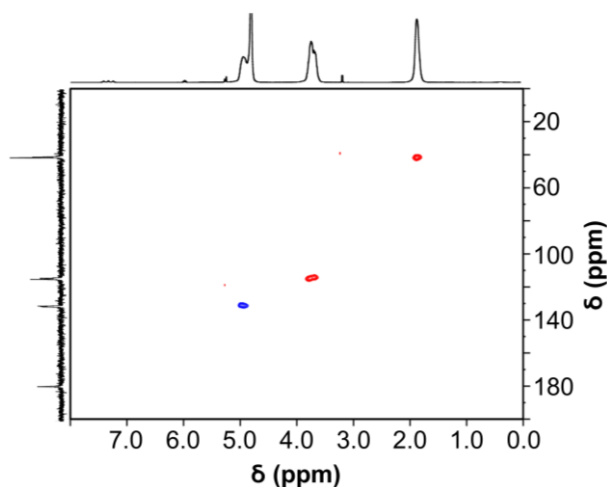


Figure S32: ^1H - ^{13}C multiplicity-edited HSQC 2D NMR spectrum of **5** in D_2O . Here, CH and CH_3 signals are highlighted in blue, whilst CH_2 signals are highlighted in red. The spectrum confirms the correlation between peaks originating from the free 3-butenoic acid and the related encapsulated peak signals, in both the ^{13}C and ^1H spectra.

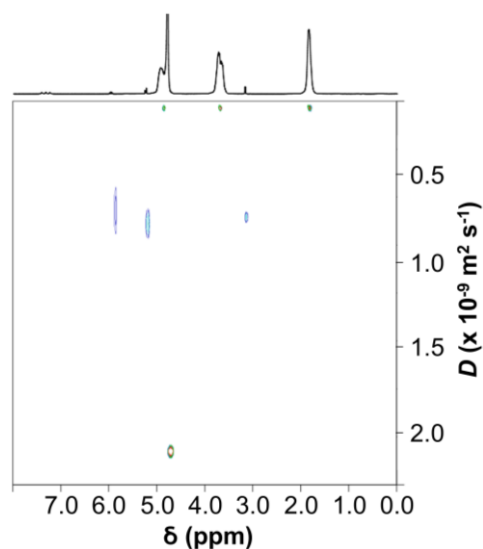


Figure S33: ^1H DOSY NMR spectrum of **5** in D_2O . The signals arising from the solvated 3-butenic acid ligand species ($\alpha\beta\gamma\text{i}$) and the encapsulated 3-butenic acid ligand species ($\alpha'\beta'\gamma'\text{i}'$) are highlighted. The solvated 3-butenic acid ligands have a diffusion coefficient of approximately $7.00 \times 10^{-10} \text{ m}^2 \text{ s}^{-1}$, whilst the encapsulated 3-butenic acid signals possess diffusion coefficients of approximately $1.10 \times 10^{-10} \text{ m}^2 \text{ s}^{-1}$. The large discrimination of the two values provides further evidence of their origins from species in two different domains.

The hydrodynamic radii of both the encapsulated and free 3-butenic acid ligand species was estimated by application of the Stokes-Einstein equation (**Equation 1**):

$$r = \frac{kT}{6\pi\eta D}$$

Where, r = van der Waals radius (m), k = Boltzmann constant ($1.380 \times 10^{-23} \text{ J K}^{-1}$), T = temperature (300 K), η = solvent viscosity (0.000853 Pa s), and D = diffusion coefficient ($\text{m}^2 \text{ s}^{-1}$). The hydrodynamic radii were determined to be $\sim 22 \text{ \AA}$ ($D = 0.000000000115 \text{ m}^2 \text{ s}^{-1}$) and $\sim 4 \text{ \AA}$ ($D = 0.000000000740 \text{ m}^2 \text{ s}^{-1}$) for the broad encapsulated peaks and the sharp free peaks, respectively.

(15) Characterization of **6** – {Mo₁₃₂(4-Pentenoic acid)}

(15.1) Thermogravimetric Analysis of **6**

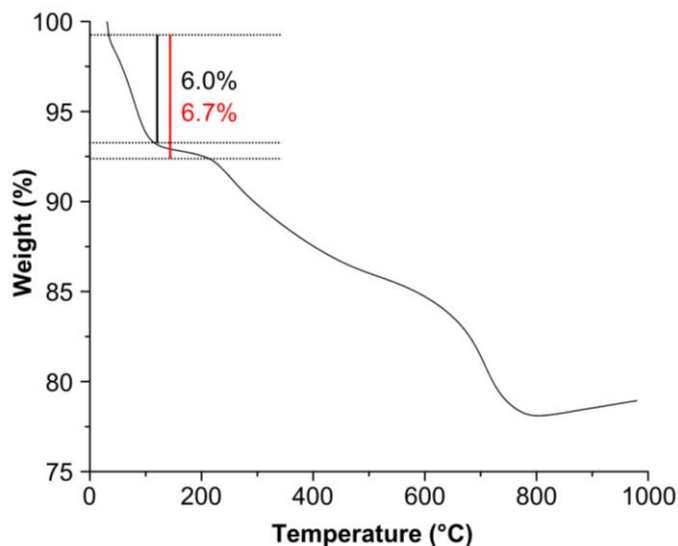


Figure S34: TGA of **6**. The percentage weight loss due to water loss between 50-225 °C is highlighted, representing approximately 90 solvent molecules.

(15.2) NMR Study of **6**

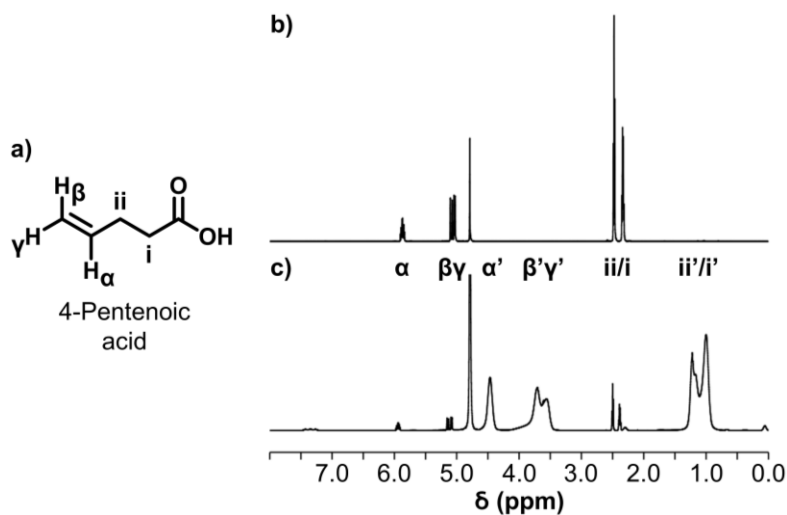


Figure S35: a) Structure of 4-pentenoic acid with labelled proton groups, b) ¹H NMR spectrum of 4-pentenoic acid in D₂O, and c) ¹H NMR spectrum of **6** in D₂O. The peaks arising from the solvated 4-pentenoic acid ligand species are highlighted: α = 6.0 ppm, β/γ = 5.1 ppm, and i/ii = 2.4 ppm. The encapsulated 4-pentenoic acid ligand species peaks appear significantly broadened and upfield shifted due to the coordination of the species to the negatively

charged $\{Mo_{132}\}$ framework, in addition to the confined nature of the ligand environment. The resultant peaks appear at $\alpha' = 4.5$ ppm, $\beta'/\gamma' = 3.6-3.7$ ppm, and $i'/ii' = 1.0-1.2$ ppm, with shifts of $\alpha-\alpha' = -1.5$ ppm, $\beta-\beta'/\gamma-\gamma' = -1.5$ ppm, and $i-i'/ii-ii' = -1.2$ ppm.

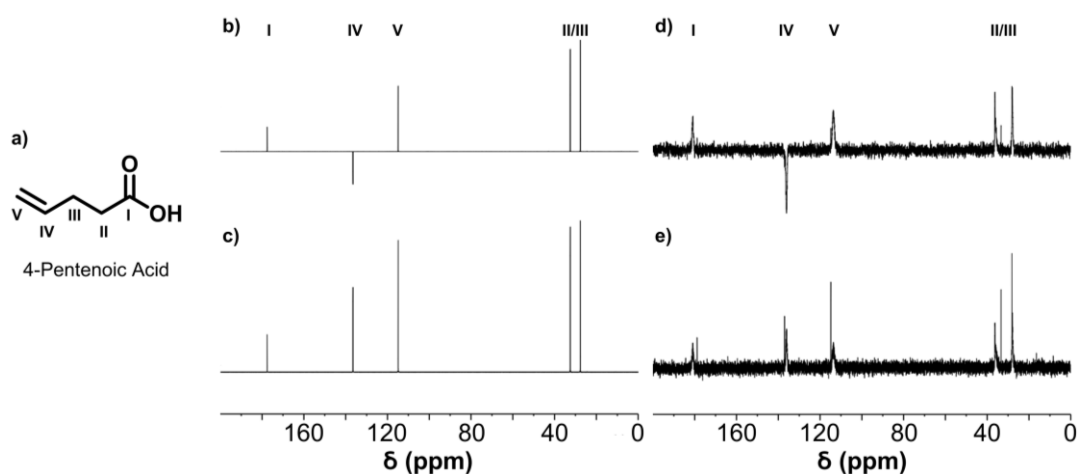


Figure S36: a) Assignment of 4-pentenoic acid for use in ^{13}C NMR spectra labelling, b) ^{13}C DEPTQ NMR spectrum of 4-pentenoic acid in D_2O , c) ^{13}C NMR spectrum of 4-pentenoic acid in D_2O , d) ^{13}C DEPTQ NMR spectrum of **6** in D_2O , and e) ^{13}C NMR spectrum of **6** in D_2O . For the ^{13}C DEPTQ NMR measurements signals arising due to quaternary carbon nuclei (C_q) and methylene (CH_2) carbon nuclei appear pointing upwards, whilst methine (CH) and methyl (CH_3) carbon nuclei appear pointing downwards. The peaks arising from the solvated 4-pentenoic ligand species are highlighted: **I** = 178 ppm ($-COO^-$), **II** = 33 ppm ($-CH_2$), **III** = 28 ppm ($-CH_2$), **IV** = 137 ppm ($-CH$), and **V** = 115 ppm ($-CH_2$). The encapsulated 4-pentenoic acid ligand species appear slightly shifted and broadened due to the same effects expressed in the 1H NMR spectra.

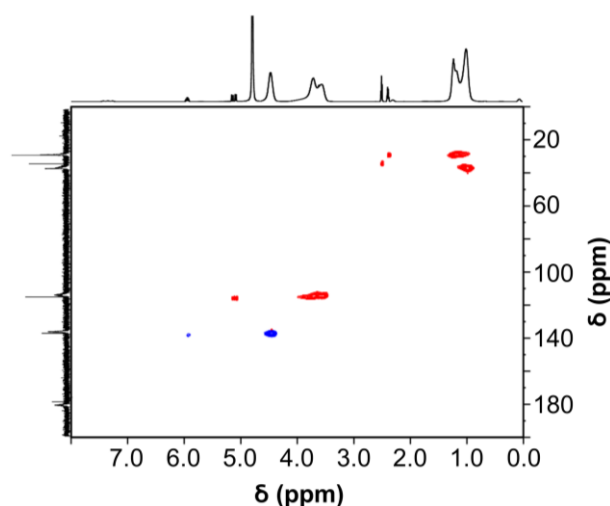


Figure S37: 1H - ^{13}C multiplicity-edited HSQC 2D NMR spectrum of **6** in D_2O . Here, CH and CH_3 signals are highlighted in blue, whilst CH_2 signals are highlighted in red. The spectrum confirms the correlation between peaks originating from the free 4-pentenoic acid and the related encapsulated peak signals, in both the ^{13}C and 1H spectra.

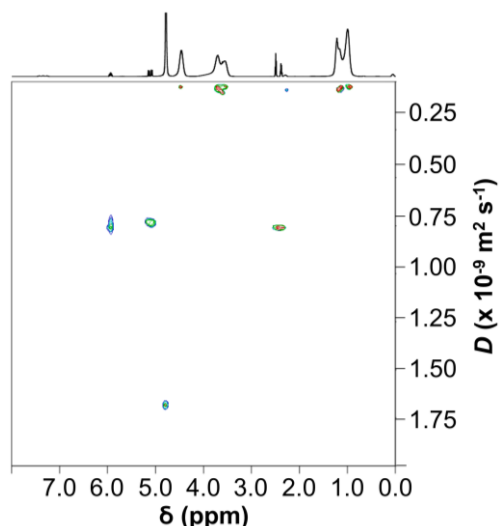


Figure S38: ^1H DOSY NMR spectrum of **6** in D_2O . The signals arising from the solvated 4-pentenoic acid ligand species ($\alpha\beta\gamma\text{ii}$) and the encapsulated 4-pentenoic acid ligand species ($\alpha'\beta'\gamma'\text{i}'\text{ii}'$) are highlighted. The solvated 4-pentenoic acid ligands have a diffusion coefficient of approximately $7.77 \times 10^{-10} \text{ m}^2 \text{ s}^{-1}$, whilst the encapsulated 4-pentenoic acid signals possess diffusion coefficients of approximately $1.14 \times 10^{-10} \text{ m}^2 \text{ s}^{-1}$. The large discrimination of the two values provides further evidence of their origins from species in two different domains. An additional peak arising from water has a diffusion coefficient of $1.66 \times 10^{-9} \text{ m}^2 \text{ s}^{-1}$.

(16) Characterization of **7** – $\{\text{Mo}_{132}(\text{5-Hexenoic Acid})\}$

(16.1) Thermogravimetric Analysis of **7**

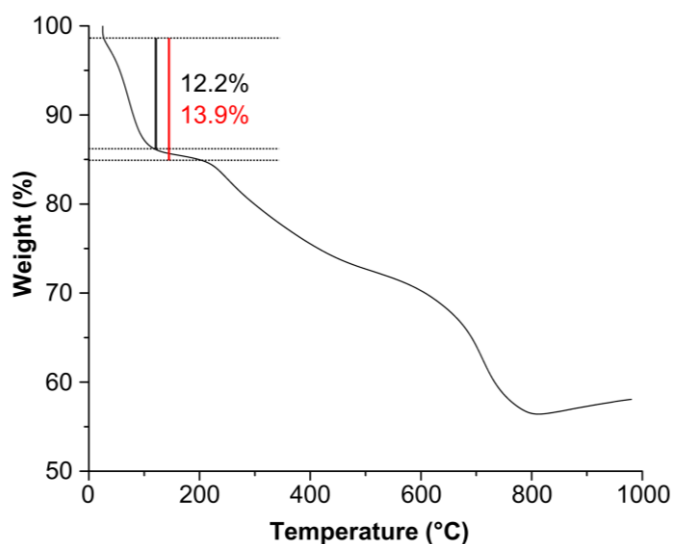


Figure S39: TGA of **7**. The percentage weight loss due to water loss between 50-225 °C is highlighted, representing approximately 200 solvent molecules.

(16.2) NMR Study of 7

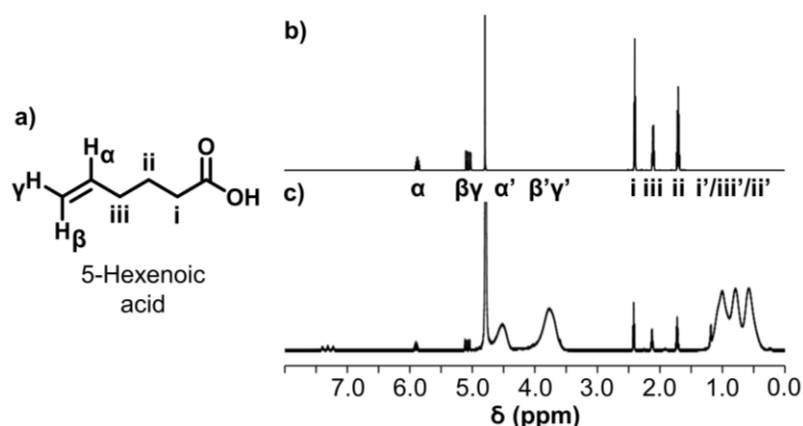


Figure S40: a) Structure of 5-hexenoic acid with labelled proton groups, b) ^1H NMR spectrum of 5-hexenoic acid in D_2O , and c) ^1H NMR spectrum of **7** in D_2O . The peaks arising from the solvated 5-hexenoic acid ligand species are highlighted: α = 5.9 ppm, β/γ = 5.1 ppm, i = 2.4 ppm, ii = 1.7 ppm, and iii = 2.1 ppm. The encapsulated 5-hexenoic acid ligand species peaks appear significantly broadened and upfield shifted due to the coordination of the species to the negatively charged $\{\text{Mo}_{132}\}$ framework, in addition to the confined nature of the ligand environment. The resultant peaks appear at α' = 4.5 ppm, β'/γ' = 3.8 ppm, i' = 1.0 ppm, ii' = 0.6 ppm, and iii' = 0.8 ppm, with shifts of $\alpha - \alpha'$ = -1.4 ppm, $\beta - \beta'/\gamma - \gamma'$ = -1.3 ppm, $i - i'$ = -1.4 ppm, $ii - ii'$ = -1.1 ppm, and $iii - iii'$ = -1.3 ppm.

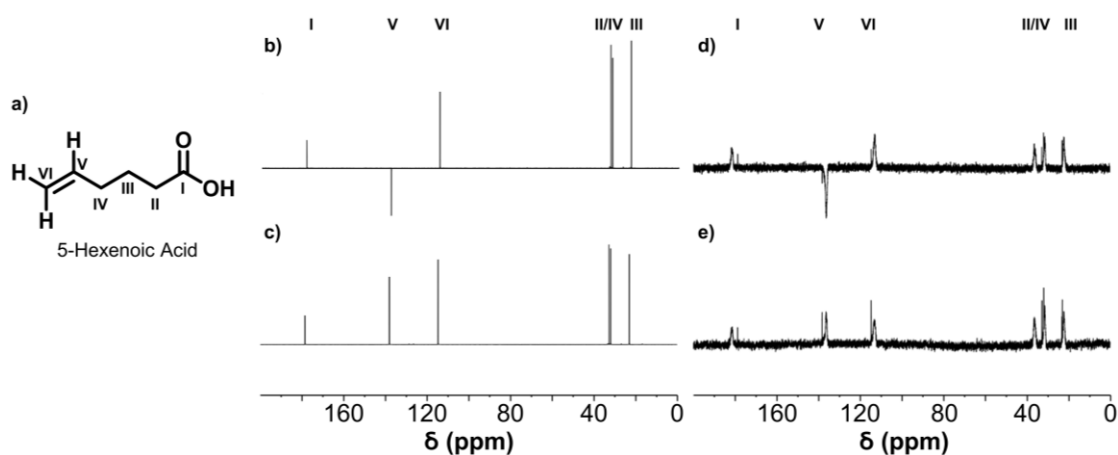


Figure S41: a) Assignment of 5-hexenoic acid for use in ^{13}C NMR spectra labelling, b) ^{13}C DEPTQ NMR spectrum of 5-hexenoic acid in D_2O , c) ^{13}C NMR spectrum of 5-hexenoic acid in D_2O , d) ^{13}C DEPTQ NMR spectrum of **7** in D_2O , and e) ^{13}C NMR spectrum of **7** in D_2O . For the ^{13}C DEPTQ NMR measurements signals arising due to quaternary carbon nuclei (C_q) and methylene (CH_2) carbon nuclei appear pointing upwards, whilst methine (CH) and methyl (CH_3) carbon nuclei appear pointing downwards. The peaks arising from the solvated 5-hexenoic acid ligand species are highlighted: **I** = 178 ppm ($-\text{COO}^-$), **II/IV** = 32 ppm ($(-\text{CH}_2)_2$), **III** = 22 ppm ($-\text{CH}_2$), **V** = 138 ppm ($-\text{CH}$),

and VI = 115 ppm (-CH₂). The encapsulated 5-hexenoic acid ligand species appear slightly shifted and broadened due to the same effects expressed in the ¹H NMR spectra.

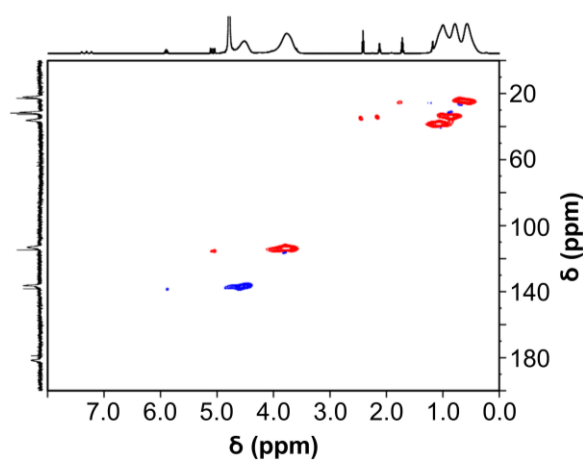


Figure S42: ¹H-¹³C multiplicity-edited HSQC 2D NMR spectrum of **7** in D₂O. Here, CH and CH₃ signals are highlighted in blue, whilst CH₂ signals are highlighted in red. The spectrum confirms the correlation between peaks originating from the free 5-hexenoic acid and the related encapsulated peak signals, in both the ¹³C and ¹H spectra.

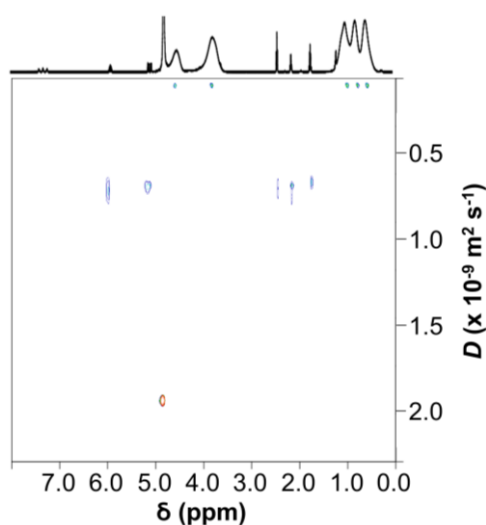


Figure S43: ¹H DOSY NMR spectrum of **7** in D₂O. The signals arising from the solvated 5-hexenoic acid ligand species ($\alpha\beta\gamma\text{ii iii}$) and the encapsulated 5-hexenoic acid ligand species ($\alpha'\beta'\gamma'\text{ii'iii'}$) are highlighted. The solvated 5-hexenoic acid ligands have a diffusion coefficient of approximately $7.02 \times 10^{-10} \text{ m}^2 \text{ s}^{-1}$, whilst the encapsulated 5-hexenoic acid signals possess diffusion coefficients of approximately $1.04 \times 10^{-10} \text{ m}^2 \text{ s}^{-1}$. The large discrimination of the two values provides further evidence of their origins from species in two different domains. An additional peak arising from water has a diffusion coefficient of $1.94 \times 10^{-9} \text{ m}^2 \text{ s}^{-1}$.

(17) Characterization of **8** – {Mo₁₃₂(Sorbic Acid)}

(17.1) Thermogravimetric Analysis of **8**

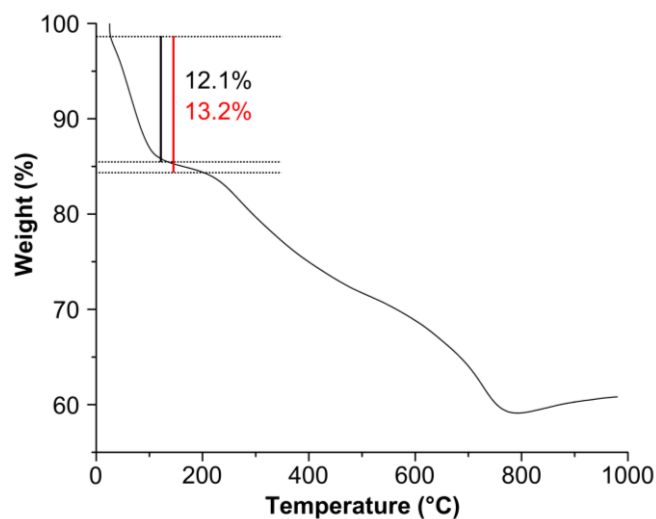


Figure S44: TGA of **8**. The percentage weight loss due to water loss between 50-225 °C is highlighted, representing approximately 190 solvent molecules.

(17.2) NMR Study of **8**

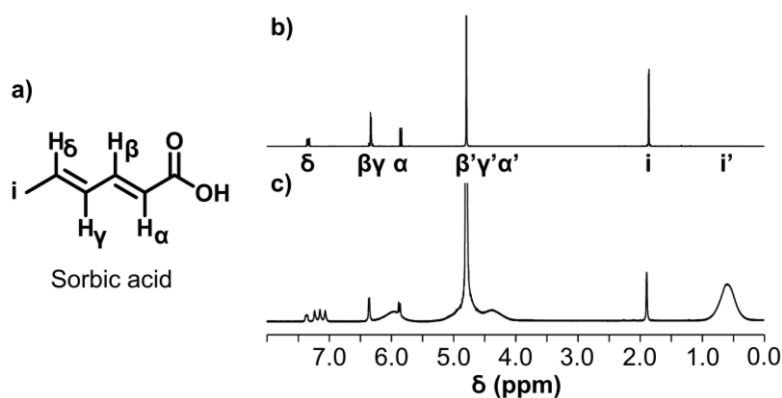


Figure S45: a) Structure of sorbic acid with labelled proton groups, b) ¹H NMR spectrum of sorbic acid in D₂O, and c) ¹H NMR spectrum of **8** in D₂O. The peaks arising from the solvated sorbic acid ligand species are highlighted: α = 5.9 ppm, β/γ = 6.4 ppm, δ = 7.4 ppm, and i = 1.9 ppm. The encapsulated sorbic acid ligand species peaks appear significantly broadened and upfield shifted due to the coordination of the species to the negatively charged {Mo₁₃₂} framework, in addition to the confined nature of the ligand environment. The resultant peaks appear at α' = 4.4 ppm,

β'/γ' both signals are obscured by the water peak at approximately 4.8 ppm, $\delta' = 5.9$ ppm, and $i' = 0.6$ ppm, with shifts of $\alpha-\alpha' = -1.5$ ppm, $\delta-\delta' = -1.6$ ppm, and $i-i' = -1.3$ ppm.

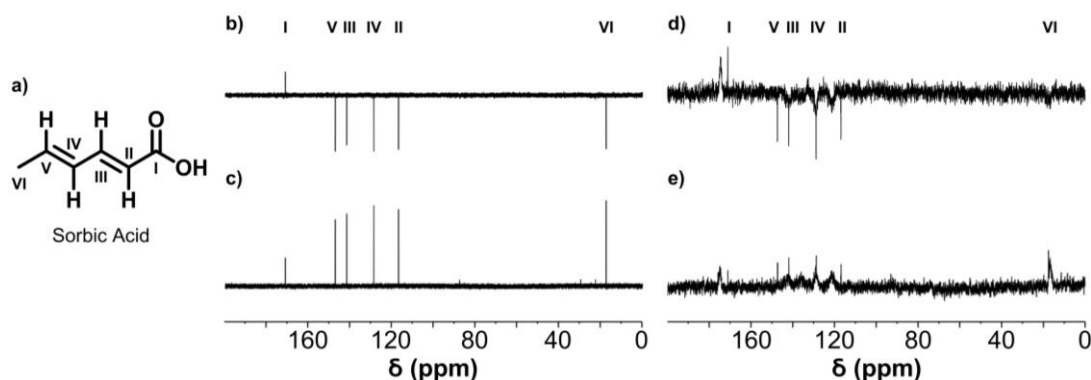


Figure S46: a) Assignment of sorbic acid for use in ^{13}C NMR spectra labelling, b) ^{13}C DEPTQ NMR spectrum of sorbic acid in D_2O , c) ^{13}C NMR spectrum of sorbic acid in D_2O , d) ^{13}C DEPTQ NMR spectrum of **8** in D_2O , and e) ^{13}C NMR spectrum of **8** in D_2O . For the ^{13}C DEPTQ NMR measurements signals arising due to quaternary carbon nuclei (C_q) and methylene (CH_2) carbon nuclei appear pointing upwards, whilst methine (CH) and methyl (CH_3) carbon nuclei appear pointing downwards. The peaks arising from the solvated sorbic ligand species are highlighted: **I** = 171 ppm ($-\text{COO}^-$), **II** = 117 ppm ($-\text{CH}$), **III** = 142 ppm ($-\text{CH}$), **IV** = 129 ppm ($-\text{CH}$), **V** = 147 ppm ($-\text{CH}$), and **VI** = 18 ppm ($-\text{CH}_3$). The encapsulated sorbic acid ligand species appear slightly shifted and broadened due to the same effects expressed in the ^1H NMR spectra.

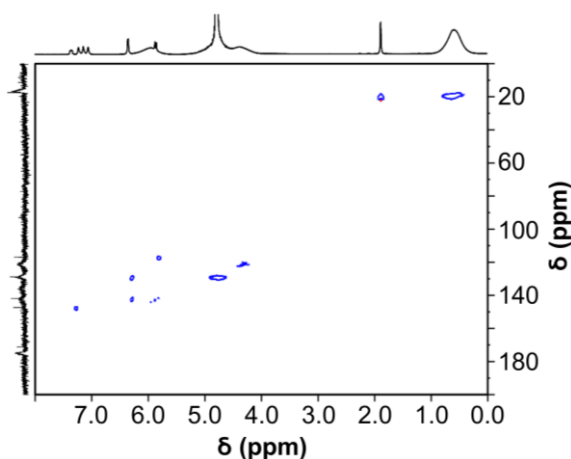


Figure S47: ^1H - ^{13}C multiplicity-edited HSQC 2D NMR spectrum of **8** in D_2O . Here, CH and CH_3 signals are highlighted in blue. The spectrum confirms the correlation between peaks originating from the free sorbic acid and the related encapsulated peak signals, in both the ^{13}C and ^1H spectra.

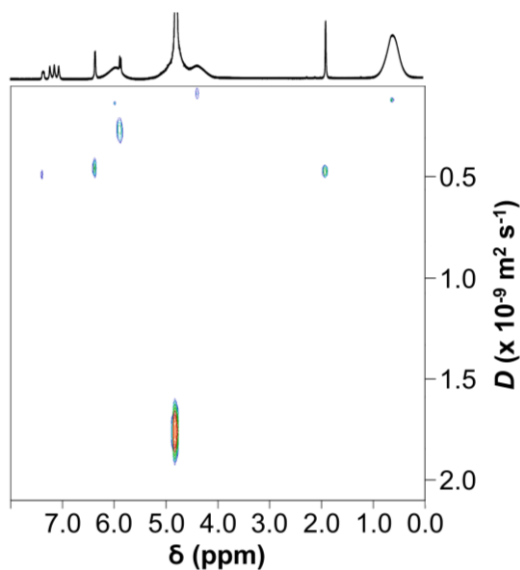


Figure S48: ^1H DOSY NMR spectrum of **8** in D_2O . The signals arising from the solvated sorbic acid ligand species ($\alpha\beta\gamma\delta\text{i}$) and the encapsulated sorbic acid ligand species ($\alpha'\beta'\gamma'\delta'\text{i}'$) are highlighted. The solvated sorbic acid ligands have a diffusion coefficient of approximately $4.66 \times 10^{-10} \text{ m}^2 \text{ s}^{-1}$, whilst the encapsulated sorbic acid signals possess diffusion coefficients of approximately $1.08 \times 10^{-10} \text{ m}^2 \text{ s}^{-1}$. The discrimination of the two values provides further evidence of their origins from species in two different domains. An additional peak arising from water has a diffusion coefficient of $1.79 \times 10^{-9} \text{ m}^2 \text{ s}^{-1}$.

(18) Thiol-containing Guest Uptake

Investigation of Uptake between Pure $\{\text{Mo}_{132}(\text{SO}_4)_{30}\}$, $\{\text{Mo}_{132}(\text{SO}_4)_{30}\}$ plus acetic acid, and $\{\text{Mo}_{132}(\text{SO}_4)_{30}\}$ plus alkene ligands, with Thiol-Containing Alkyl Guests

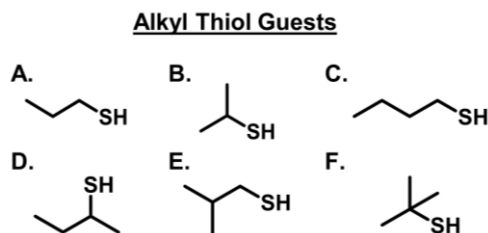


Figure S49: Guests used for encapsulation studies: propanethiol (**A**), 2-propanethiol (**B**), 1-butanethiol (**C**), 2-butanethiol (**D**), 2-methyl-1-propanethiol (**E**), and 2-methyl-2-propanethiol.

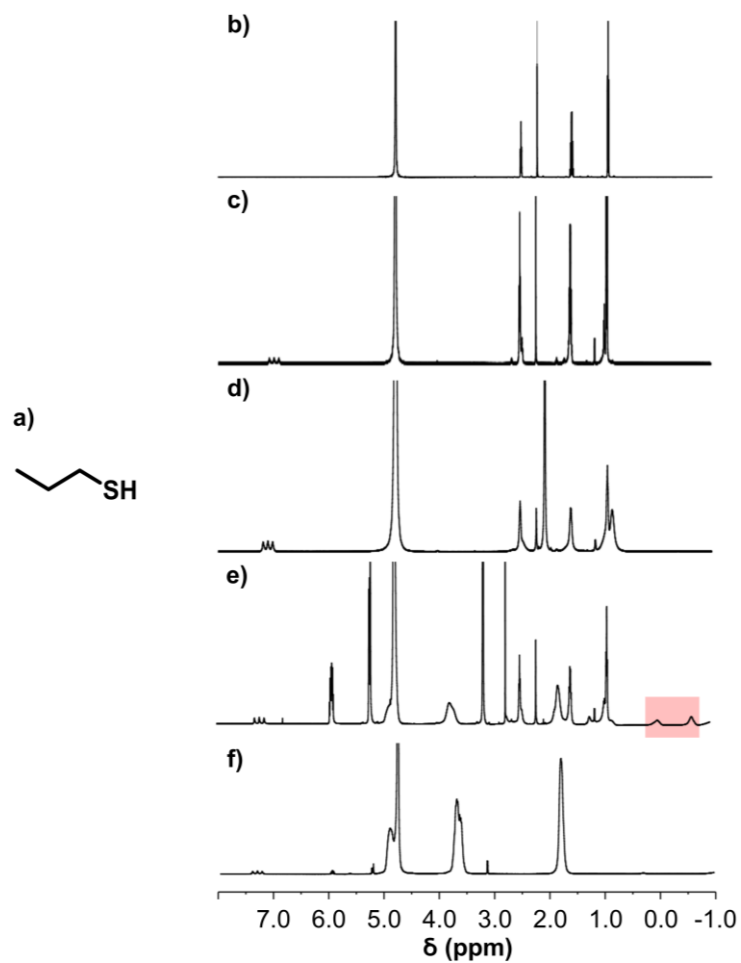


Figure S50: a) Structure of 1-propanethiol, and ^1H NMR spectra of b) pure 1-propanethiol, c) $\{\text{Mo}_{132}(\text{SO}_4)_{30}\}$ with added 1-propanethiol, d) $\{\text{Mo}_{132}(\text{SO}_4)_{30}\}$ and OAc (60 equivalents) with added 1-propanethiol, e) **5** with added 1-propanethiol with a methanesulfonic acid external reference (2.8 ppm), and f) **5** in D_2O . A broad peak related to the encapsulation of the 1-propanethiol guest is highlighted by the red box for **5**.

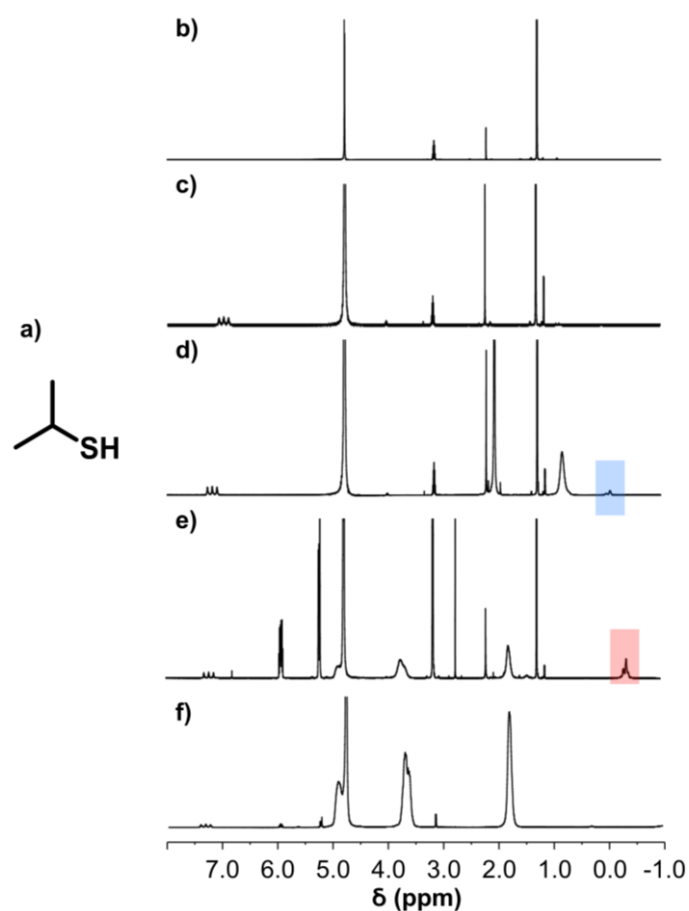


Figure S51: a) Structure of 2-propanethiol, and ^1H NMR spectra of b) pure 2-propanethiol, c) $\{\text{Mo}_{132}(\text{SO}_4)_{30}\}$ with added 2-propanethiol, d) $\{\text{Mo}_{132}(\text{SO}_4)_{30}\}$ and OAc (60 equivalents) with added 2-propanethiol, e) **5** with added 2-propanethiol with a methanesulfonic acid external reference (2.8 ppm), and f) **5** in D_2O . A broad peak related to the encapsulation of the 2-propanethiol guest is highlighted by the red box for **5** and a blue box for $\{\text{Mo}_{132}(\text{OAc})_{30}\}$.

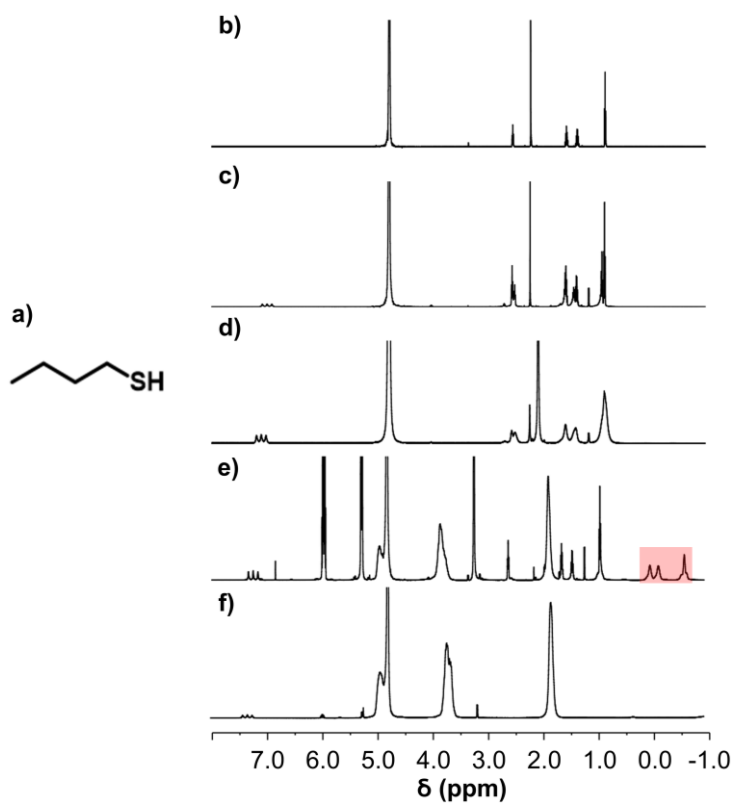


Figure S52: a) Structure of 1-butanethiol, and ^1H NMR spectra of b) pure 1-butanethiol, c) $\{\text{Mo}_{132}(\text{SO}_4)_{30}\}$ with added 1-butanethiol, d) $\{\text{Mo}_{132}(\text{SO}_4)_{30}\}$ and OAc (60 equivalents) with added 1-butanethiol, e) **5** with added 1-butanethiol with a methanesulfonic acid external reference (2.8 ppm), and f) **5** in D_2O . A broad peak related to the encapsulation of the 1-butanethiol guest is highlighted by the red box for **5**.

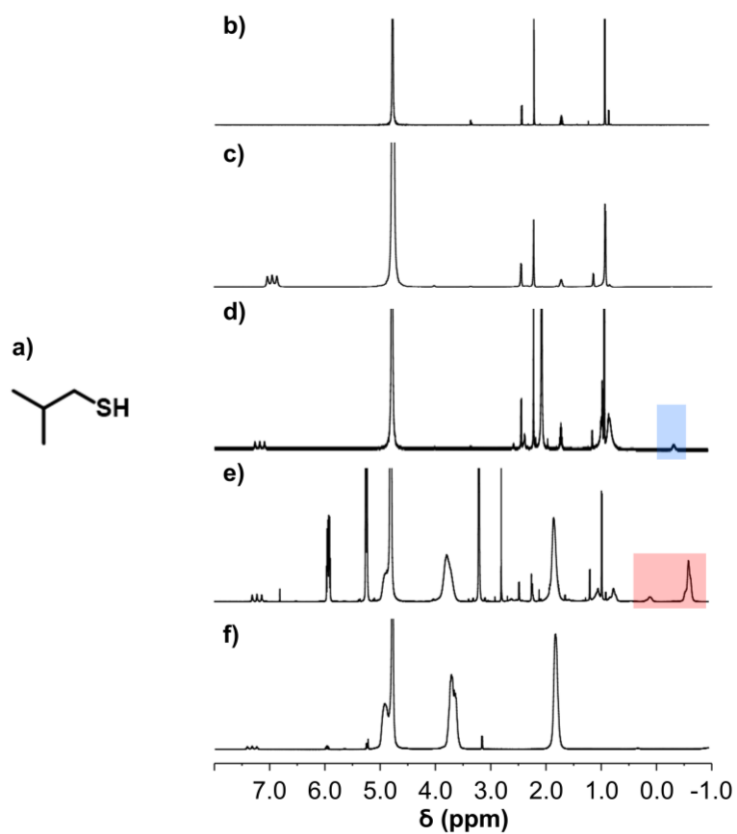


Figure S53: a) Structure of 2-methyl-1-propanethiol, and ^1H NMR spectra of b) pure 2-methyl-1-propanethiol, c) $\{\text{Mo}_{132}(\text{SO}_4)_{30}\}$ with added 2-methyl-1-propanethiol, d) $\{\text{Mo}_{132}(\text{SO}_4)_{30}\}$ and OAc (60 equivalents) with added 2-methyl-1-propanethiol, e) **5** with added 2-methyl-1-propanethiol with a methanesulfonic acid external reference (2.8 ppm), and f) **5** in D_2O . A broad peak related to the encapsulation of the 2-methyl-1-propanethiol guest is highlighted by the red box for **5** and a blue box for $\{\text{Mo}_{132}(\text{OAc})_{30}\}$.

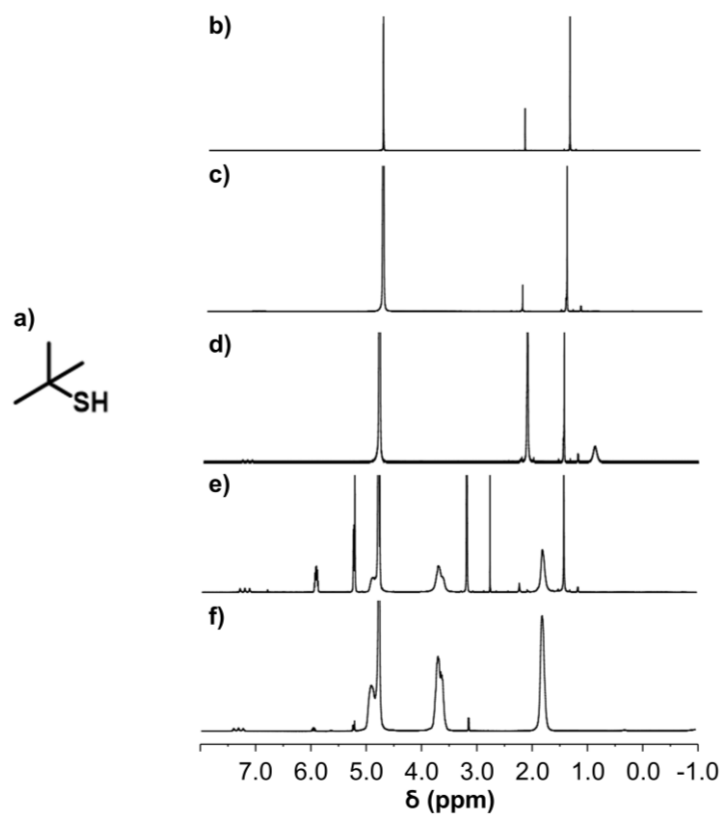


Figure S54: a) Structure of 2-methyl-2-propanethiol, and ^1H NMR spectra of b) pure 2-methyl-2-propanethiol, c) $\{\text{Mo}_{132}(\text{SO}_4)_{30}\}$ with added 2-methyl-2-propanethiol, d) $\{\text{Mo}_{132}(\text{SO}_4)_{30}\}$ and OAc (60 equivalents) with added 2-methyl-2-propanethiol, e) **5** with added 2-methyl-2-propanethiol with a methanesulfonic acid external reference (2.8 ppm), and f) **5** in D_2O .

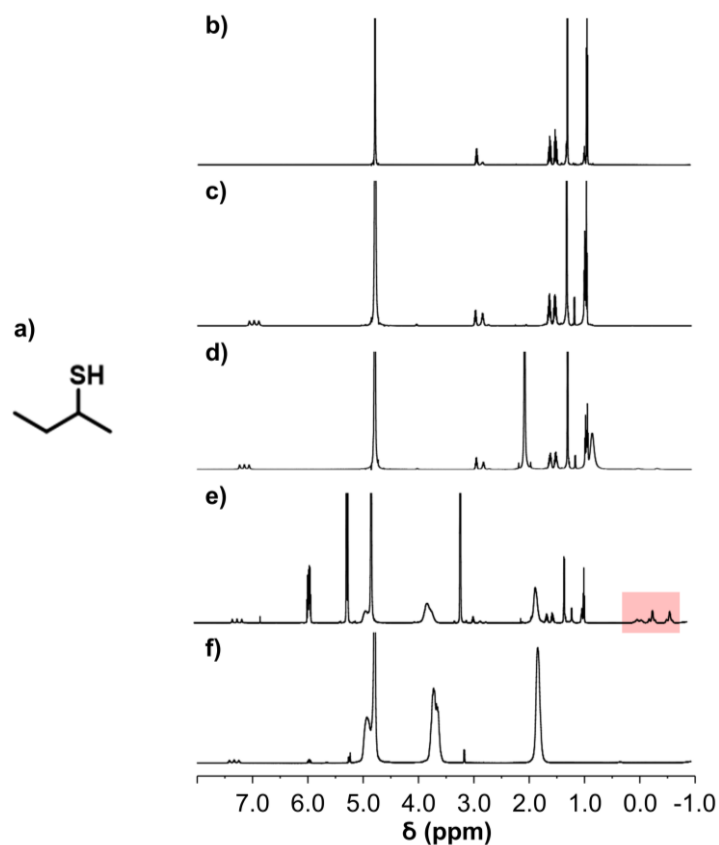


Figure S55: a) Structure of 2-butanethiol, and ^1H NMR spectra of b) pure 2-butanethiol, c) $\{\text{Mo}_{132}(\text{SO}_4)_{30}\}$ with added 2-butanethiol, d) $\{\text{Mo}_{132}(\text{SO}_4)_{30}\}$ and OAc (60 equivalents) with added 2-butanethiol, e) **5** with added 2-butanethiol with a methanesulfonic acid external reference (2.8 ppm), and f) **5** in D_2O . A broad peak related to the encapsulation of the 2-butanethiol guest is highlighted by the red box for **2**.

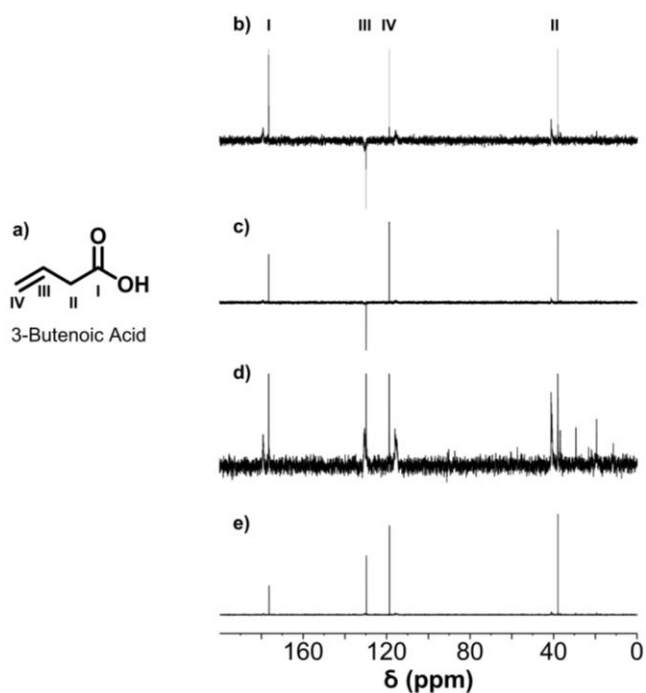


Figure S56: a) Assignment of 3-butenic acid for use in ^{13}C NMR spectra labelling, b) enhanced ^{13}C DEPTQ NMR spectrum of $\{\text{Mo}_{132}(\text{SO}_4)_{30}\}$ plus 3-butenic acid and 1-butanethiol in D_2O , c) ^{13}C DEPTQ NMR spectrum of $\{\text{Mo}_{132}(\text{SO}_4)_{30}\}$ plus 3-butenic acid and 1-butanethiol in D_2O , d) enhanced ^{13}C NMR spectrum of $\{\text{Mo}_{132}(\text{SO}_4)_{30}\}$ plus 3-butenic acid and 1-butanethiol in D_2O , and e) ^{13}C NMR spectrum of $\{\text{Mo}_{132}(\text{SO}_4)_{30}\}$ plus 3-butenic acid and 1-butanethiol in D_2O . For the ^{13}C DEPTQ NMR measurements signals arising due to quaternary carbon nuclei (C_q) and methylene (CH_2) carbon nuclei appear pointing upwards, whilst methine (CH) and methyl (CH_3) carbon nuclei appear pointing downwards. The peaks arising from the solvated 3-butenic acid ligand species are highlighted: **I** = 179 ppm ($-\text{COO}^-$), **II** = 40 ppm ($-\text{CH}$), **III** = 130 ppm ($-\text{CH}_2$), and **IV** = 114 ppm ($-\text{CH}_2$). The encapsulated 3-butenic acid ligand species appear slightly shifted and broadened due to the same effects expressed in the ^1H NMR spectra. Additional peaks related to the 1-butanethiol species are present between 10-30 ppm, as seen in **d**).

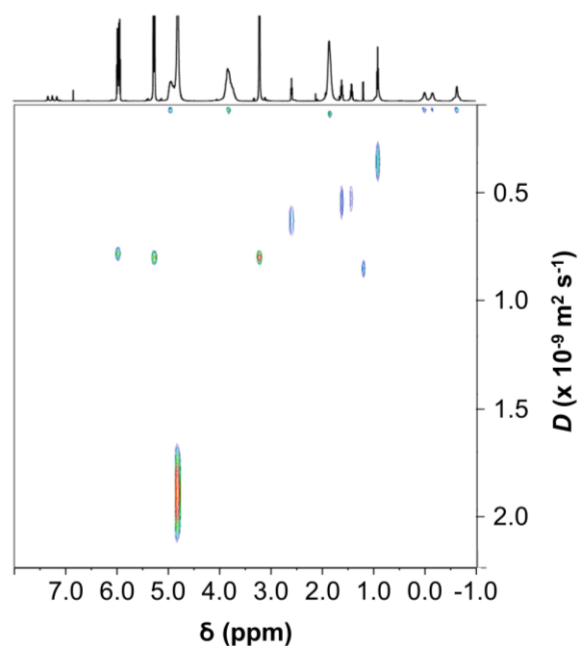


Figure S57: ^1H DOSY NMR spectrum of $\{\text{Mo}_{132}(\text{SO}_4)_{30}\}$ plus 3-butenic acid and 1-butanethiol in D_2O . The previously assigned solvated 3-butenic acid ligands have a diffusion coefficient of approximately $7.95 \times 10^{-10} \text{ m}^2 \text{ s}^{-1}$, whilst the encapsulated 3-butenic acid signals possess diffusion coefficients of approximately $1.30 \times 10^{-10} \text{ m}^2 \text{ s}^{-1}$. Further, the peaks assigned to solvated 1-butanethiol possess diffusion coefficients of approximately $5.35 \times 10^{-10} \text{ m}^2 \text{ s}^{-1}$, whilst those signals assigned to encapsulated 1-butanethiol possess diffusion coefficients of approximately $1.28 \times 10^{-10} \text{ m}^2 \text{ s}^{-1}$. The close approximation of values for the encapsulated guest species and ligand species indicates that the two separate species are present in a similar environment, the inner cavity of the $\{\text{Mo}_{132}\}$ structure. An additional peak arising from water has a diffusion coefficient of $1.88 \times 10^{-9} \text{ m}^2 \text{ s}^{-1}$.

Table S6 Number of thiol guests (A to F) encapsulated within the $\{\text{Mo}_{132}(\text{SO}_4)_{30}\}$ cavity with added alkene ligands.

	Thiol Guest	1-Propanethiol	2-Propanethiol	1-Butanethiol	2-Butanethiol	2-Methyl-1-propanethiol	2-Methyl-2-propanethiol
Alkene Ligand	Label	A	B	C	D	E	F
Acrylic acid	1	27.3	8.6	24.0	20.2	21.7	2.1
3-Butenoic acid	5	7.0	16.5	16.0	22.2	18.2	0.0
4-Pentenoic acid	6	9.5	9.4	7.5	7.3	7.6	0.0
5-Hexenoic acid	7	5.0	3.5	5.9	2.6	5.8	0.0

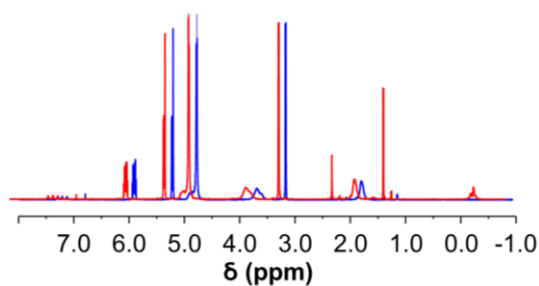


Figure S58: ^1H NMR of $\{\text{Mo}_{132}(\text{SO}_4)_{30}\}$ plus 3-butenic acid (blue spectrum), and $\{\text{Mo}_{132}(\text{SO}_4)_{30}\}$ plus 3-butenic acid and 1-propanethiol (red spectrum), in D_2O , to compare the effects of thiol encapsulation upon alkene encapsulation. The latter spectrum has been shifted downfield slightly to resolve the individual peaks of the two spectra more clearly.

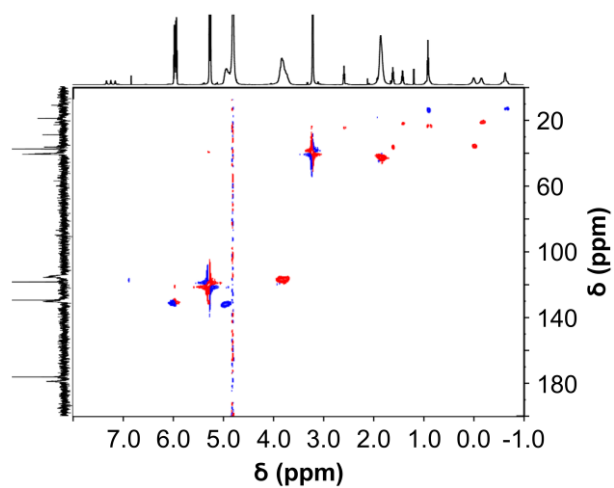


Figure S59: ^1H - ^{13}C multiplicity-edited HSQC 2D NMR spectrum of $\{\text{Mo}_{132}(\text{SO}_4)_{30}\}$ plus 3-butenic acid and 1-butanethiol in D_2O . Here, CH and CH_3 signals are highlighted in blue, whilst CH_2 signals are highlighted in red. The spectrum confirms the previously assigned encapsulated 1-butanethiol peaks in both the ^{13}C and ^1H spectra.

Investigation of Increasing Temperature on Uptake of 1-butanethiol with $\{Mo_{132}(SO_4)_{30}\}$ plus 3-butenic acid

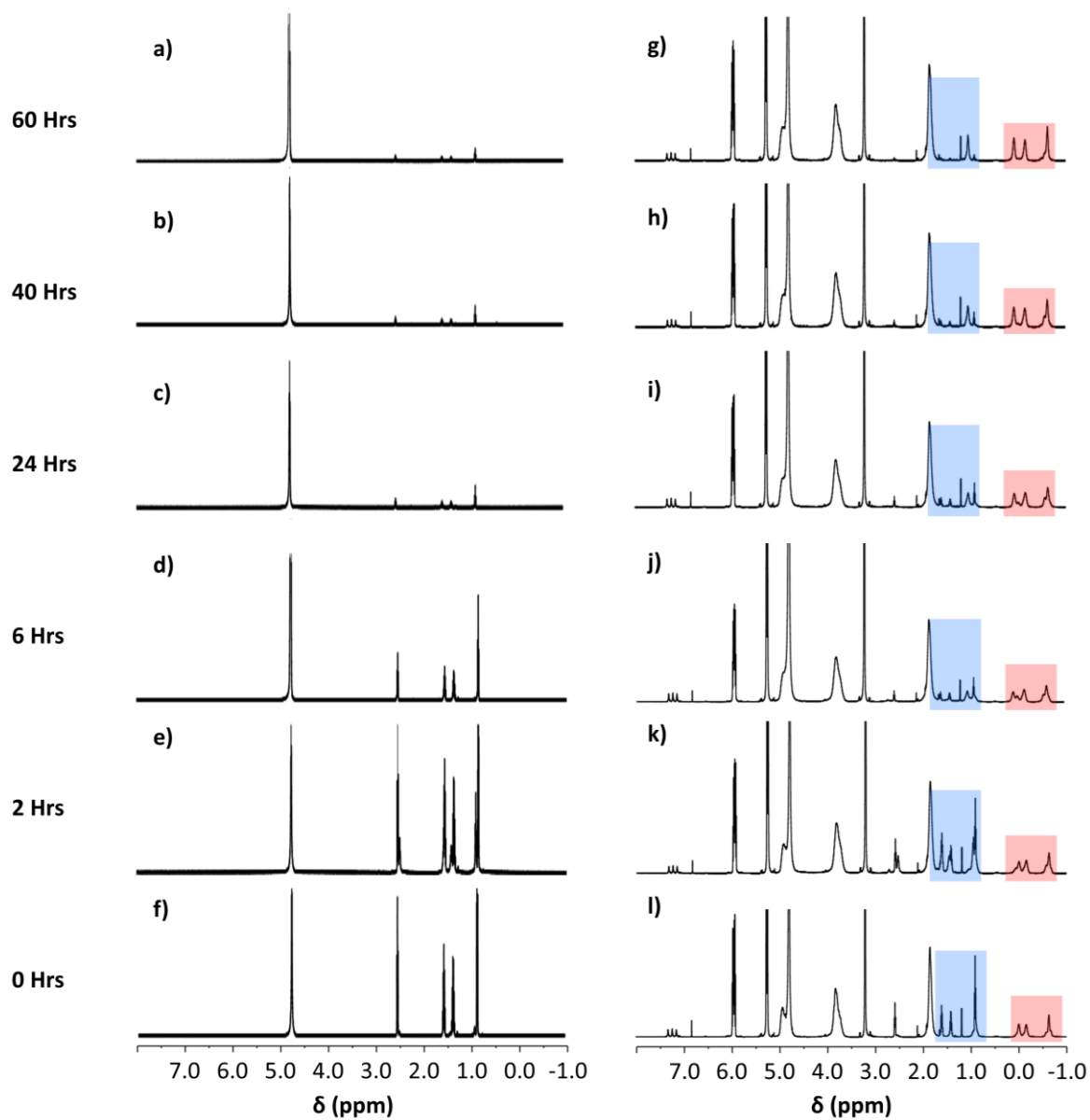


Figure S60: 1H NMR spectra of 1-butanethiol (a) – f) and 1-butanethiol with $\{Mo_{132}(SO_4)_{30}\}$ and added 3-butenic acid (g) – l), over a 60-hour period of heating at 70 °C.

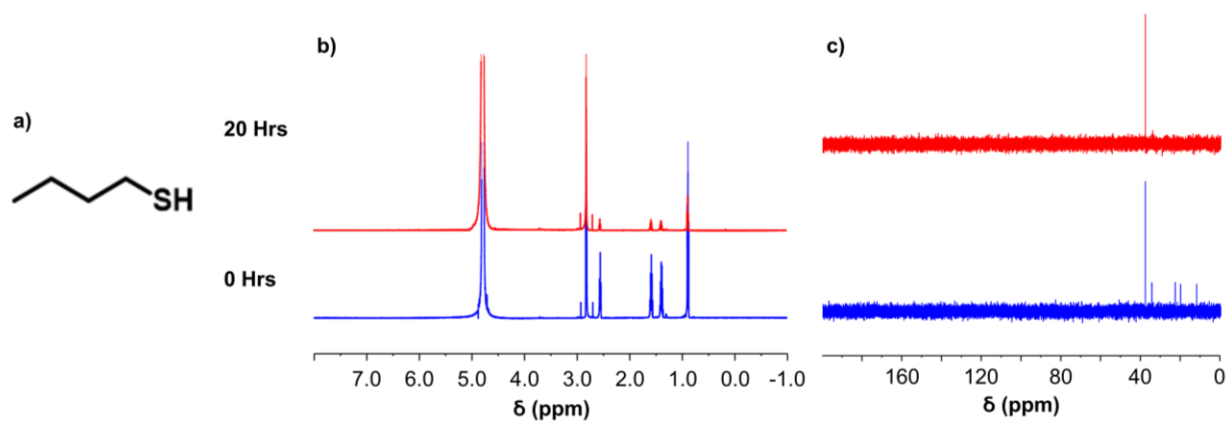


Figure S61: a) Structure of 1-butanethiol, b) ^1H NMR spectra of 1-butanethiol at 300 K prior to and post heating at 343 K for 20 hours, and c) ^{13}C NMR spectra for the same sample under the same conditions. A clear decrease in peak intensity is observed in both spectra (see peaks in the regions at 1.4-1.6 ppm and 10-38 ppm for the ^1H and ^{13}C NMR spectra).

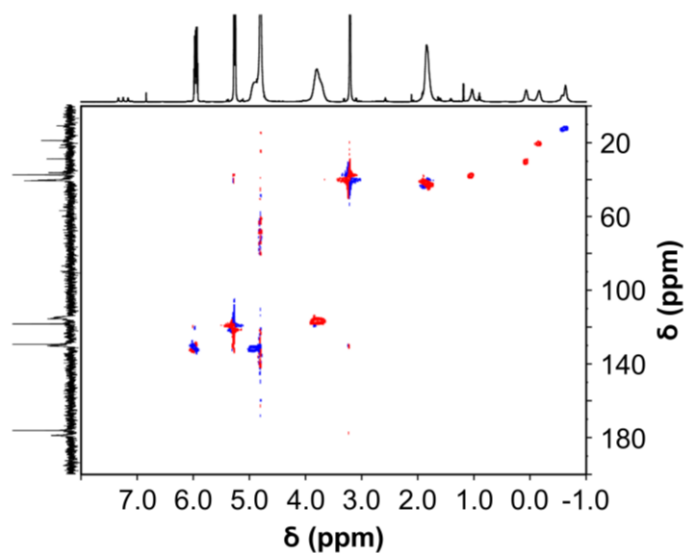


Figure S62: ^1H - ^{13}C multiplicity-edited HSQC 2D NMR spectrum of $\{\text{Mo}_{132}(\text{SO}_4)_{30}\}$ plus 3-butenioic acid and 1-butanethiol in D_2O , after heating to 343 K for 60 hours. Here, CH and CH_3 signals are highlighted in blue, whilst CH_2 signals are highlighted in red. The spectrum confirms the previously assigned encapsulated 1-butanethiol peaks are retained after the heating process has completed, whilst the free thiol species peaks have disappeared.

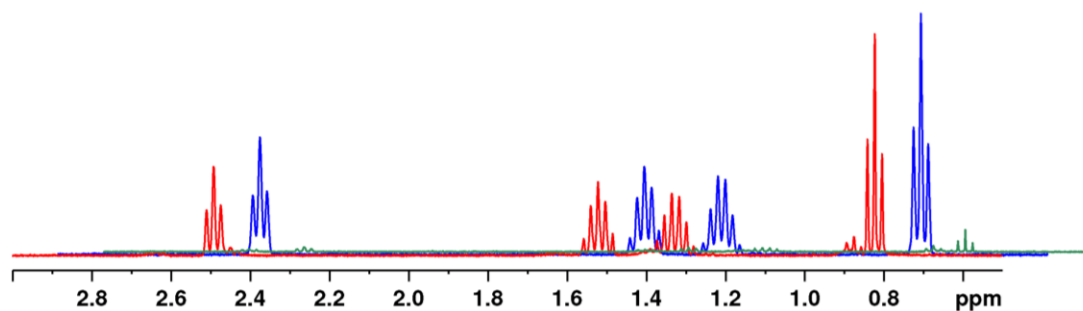


Figure S63: ^1H NMR of pure 1-butanethiol in D_2O prior to heating (red spectrum), after heating to 344 K for 40 hours in a screw cap NMR tube (blue spectrum), and after heating to 344 K for a further 20 hours in an uncapped NMR tube (green spectrum). The latter two spectra have been shifted upfield slightly to resolve the individual peaks more clearly.

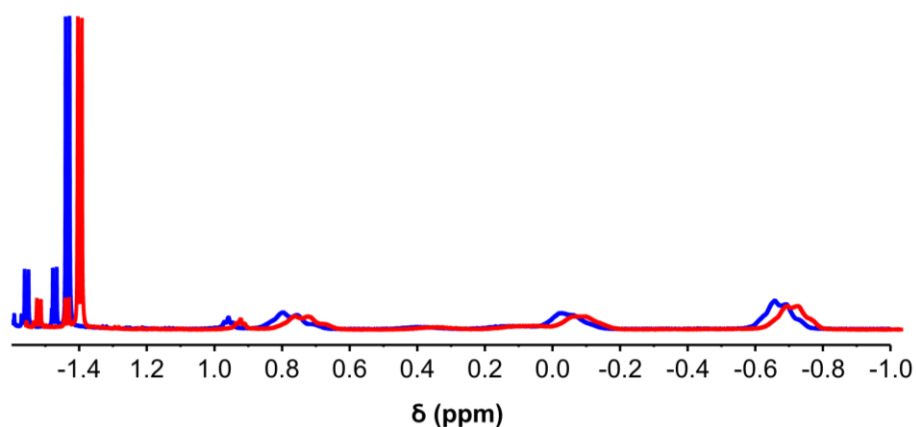


Figure S64: ^1H NMR of $\{\text{Mo}_{132}(\text{SO}_4)_{30}\}$ plus 3-butenic acid and 1-propanethiol prior to heating (blue spectrum), and $\{\text{Mo}_{132}(\text{SO}_4)_{30}\}$ plus 3-butenic acid and 1-propanethiol after heating to 368 K for 60 minutes (red spectrum), in D_2O . The latter spectrum has been shifted upfield slightly to resolve the individual peaks of the two spectra more clearly.

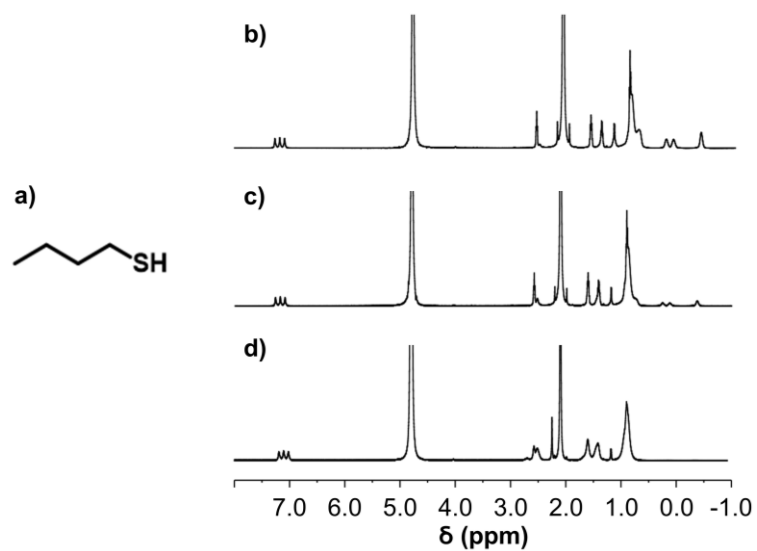


Figure S65: a) Structure of 1-butanethiol, and ^1H NMR spectra of 1-butanethiol plus $\{\text{Mo}_{132}(\text{SO}_4)_{30}\}$ with added acetate ligands in b) 120, c) 90, and d) 60 equivalents. Peaks arising due to the encapsulation of 1-butanethiol within the central cavity of $\{\text{Mo}_{132}\}$ are observed between 0.3 to -0.5 ppm for the spectra with 90 and 120 equivalents of acetate ligands added.

References

1. A. Müller, E. Krickemeyer, H. Bögge, M. Schmidtman, and F. Peters, *Angew. Chem., Int. Ed.*, 1998, **37** (24), 3360-3363.
2. S. Floquet, E. Terazzi, A. Hizaji, L. Guénée, C. Piguet, and E. Cadot, *New J. Chem.*, 2012, **36**, 865-868.
3. N. Watfa, S. Floquet, E. Terazzi, W. Salomon, L. Guénée, K. L. Buchwalder, A. Hijazi, D. Naoufal, C. Piguet, and E. Cadot, *Inorganics*, 2015, **3**, 246-266.
4. O. Petina, D. Rehder, E. T. K. Haupt, A. Grego, I. A. Weinstock, A. Merca, H. Bögge, J. Szakács, and A. Müller, *Angew. Chem., Int. Ed.*, 2011, **50**, 410-414.
5. R. Fareghi-Alamdari, N. Zekri, A. J. Moghadam, and M. R. Farsani, *Catalysts Communications*, 2017, **98**, 71-75.
6. A. Müller, S. K. Das, S. Talismanov, S. Roy, E. Beckmann, H. Bögge, M. Schmidtman, A. Merca, A. Berkle, L. Allouche, Y. Zhou, and L. Zhang, *Angew. Chem., Int. Ed.*, 2003, **42**, 5039-5044.
7. A. Müller, Y. Zhou, H. Bögge, M. Schmidtman, T. Mitra, E. T. K. Haupt, and A. Berkle, *Angew. Chem., Int. Ed.*, 2006, **45**, 460-465.
8. A. Müller, D. Rehder, E. T. K. Haupt, A. Merca, H. Bögge, M. Schmidtman, and G. Heinze-Brückner, *Angew. Chem., Int. Ed.*, 2004, **43**, 4466-4470.
9. A. Merca, E. T. K. Haupt, T. Mitra, H. Bögge, D. Rehder, and A. Müller, *Chem. - Eur. J.*, 2007, **13**, 7650-7658.
10. A. Müller, Y. Zhou, L. Zhang, H. Bögge, M. Schmidtman, M. Dressel, and J. V. Slageren, *Chem. Commun.*, 2004, 2038-2039.
11. L. Zhang, Y. Zhou, and R. Han, *Eur. J. Inorg. Chem.*, 2010, **17**, 2471-2475.
12. A. Müller, L. Toma, H. Bögge, C. Schäffer, and A. Stammer, *Angew. Chem., Int. Ed.*, 2005, **44**, 7757-7761.
13. A. Merca, H. Bögge, M. Schmidtman, Y. Zhou, E. T. K. Haupt, M. K. Sarker, C. L. Hill, and A. Müller, *Chem. Commun.*, 2008, **8**, 948-950.
14. A. Müller, E. Krickemeyer, H. Bögge, M. Schmidtman, B. Botar, and M. O. Talismanova, *Angew. Chem., Int. Ed.*, 2003, **42**, 2085-2090.
15. T. Mitra, P. Miró, A.-R. Tomsa, A. Merca, H. Bögge, J. B. Ávalos, J. M. Poblet, C. Bo, and A. Müller, *Chem. - Eur. J.* 2009, **15**, 1844-1852.
16. S. Garai, E. T. K. Haupt, H. Bögge, A. Merca, and A. Müller, *Angew. Chem.*, 2012, **124**, 10680-10683.

17. A. Müller, L. Toma, H. Bögge, M. Henry, E. T. K. Haupt, A. Mix, and F. L. Sousa, *Chem. Commun.*, 2006, 3396-3398.
18. C. Schäffer, A. M. Todea, H. Bögge, O. A. Petina, D. Rehder, E. T. K. Haupt, and A. Müller, *Chem. - Eur. J.*, 2011, **17**, 9634-9639.
19. C. Schäffer, H. Bögge, A. Merca, I. A. Weinstock, D. Rehder, E. T. K. Haupt, and A. Müller, *Angew. Chem., Int. Ed.*, 2009, **48**, 8051-8056.
20. A. Ziv, A. Grego, S. Kopilevich, L. Zeiri, P. Miro, C. Bo, A. Müller, and I. A. Weinstock, *J. Am. Chem. Soc.*, 2009, **131**, 6380-6382.
21. M. Awada, S. Floquet, J. Marrot, M. Haouas, S. P. Morcillo, C. Bour, V. Gandon, V. Coeffard, C. Greck, and E. Cadot, *J. Clust. Sci.*, 2017, **28**, 799-812.
22. T.-L. Lai, M. Awada, S. Floquet, C. Roch-Marchal, N. Watfa, J. Marrot, M. Haouas, F. Taulelle, and E. Cadot, *Chem. - Eur. J.*, 2015, **21**, 13311-13320.
23. G. M. Sheldrick, *Acta Crystallogr. Sect. A Found. Crystallogr.*, 1990, **46 (6)**, 467.
24. R. Herbst-Irmer, and G. M. Sheldrick, *Acta Crystallogr. Sect. B. Struct. Sci.* 1998, **54 (4)**, 443.
25. L. J. Farrugia, *J. Appl. Crystallogr.*, 1999, **32 (4)**, 837.
26. A. Müller, E. Krickemeyer, H. Bögge, M. Schmidtman, B. Botar, and M. O. Talismanova, *Angew. Chem., Int. Ed.*, 2003, **42**, 2085-2090.
27. F. M. Wampler, *Plant/Oper. Prog.*, 1988, **7**, 183-189.